China Geology 8 (2025) 141−158

China Geology

Journal homepage: http://chinageology.cgs.cn
https://www.sciencedirect.com/journal/china-geology

Mesozoic multi-direction collision tectonic evolution of the Ordos Basin, China: Insights from the detrital zircon and apatite (U-Th)/He analyses

Yin Chen[a, b,*], Jian-guo Li[c,*], Lu-lu Chen[a, b, d], Hua-lei Zhao[a, b]

[a] *Tianjin Center of China Geological Survey*, *Tianjin* 300170, *China*
[b] *Key Laboratory of Uranium Geology*, *China Geological Survey*, *Tianjin* 300170, *China*
[c] *Cores and Samples Center of Natural Resources*, *China Geological Survey*, *Langfang* 065201, *China*
[d] *Key Laboratory of Tectonics and Petroleum Resources*, *China University of Geosciences (Wuhan)*, *Wuhan* 430074, *China*

ARTICLE INFO

Article history:
Received 21 November 2022
Received in revised form 13 September 2023
Accepted 19 September 2023
Available online 13 January 2024

Keywords:
Zircon and Apatite (U-Th)/He
Tectonic evolution
Geochronology
Four stages of regional tectonic
Ordos Basin
Oil-gas-bearing basin
Multi-direction collision
Oil-gas exploration engineering
Mesozoic
North China Craton

ABSTRACT

The Ordos Basin (OB) in the western part of the North China Craton (NCC), was located at the jointed area of multi-plates and has recorded the Mesozoic tectonic characteristics. Its tectonic evolution in the Mesozoic is significant to understand the tectonic transformation of the northern margin of the NCC. In this work, the detrital zircon and apatite (U-Th)/He chronological system were analyzed in the northern part of the OB, and have provided new evidence for the regional tectonic evolution. The (U-Th)/He chronological data states the weighted ages of 240–235 Ma, 141 Ma with the peak distribution of 244 Ma, 219 Ma, 173 Ma, 147–132 Ma. The thermal evolution, geochronological data, and regional unconformities have proved four stages of regional tectonic evolution for the OB and its surroundings in the Mesozoic: (1) The Late Permian-Early Triassic; (2) the Late Triassic-Early Jurassic; (3) the Late Jurassic-Early Cretaceous; (4) the Late Cretaceous-Early Paleogene. It is indicated that the multi-directional convergence from the surrounding tectonic units has controlled the Mesozoic tectonic evolution of the OB. Four-stage tectonic evolution reflected the activation or end of different plate movements and provided new time constraints for the regional tectonic evolution of the NCC in the Mesozoic.

1. Introduction

The Ordos Basin (OB) located in the western part of the North China Craton (NCC), has experienced the multi-stage tectonic evolution in the Mesozoic with a series of energy resources (Liu CY et al., 2006; Chen G et al., 2007; Ren ZL et al., 2020; Yu RA et al., 2021; Chen Y et al., 2022). It was surrounded by the Yinshan-Yanshan Orogenic Belt (YOB), Taihang-Lüliang Orogenic Belt (TLOB), Qilian-Qinling-Dabie Orogenic Belt (QOB), and Liupanshan-Helanshan Orogenic Belt (Fig. 1). Multiple energy resources, such as oil/gas, coal, and uranium, are abundant and co-existing in the basin (Deng J et al., 2005; Liu CY et al., 2006, 2009). The studies on the Mesozoic evolution of the OB are significant to understand the tectonic transformation of the NCC and the ore-forming process of energy resources.

Due to the exploration of muti-energy resources, the lithostratigraphy structures, subsidence-uplift histories, and tectonic evolution of the OB in the Mesozoic have been investigated (Liu CY et al., 2006, 2009; Zhang YQ et al., 2006, 2007; Ren ZL et al., 2020; Jin RS et al., 2020a). The regional unconformities indicated the OB has experienced seven episodes of tectonic events in the Mesozoic (Jin RS et al., 2020b; Wang SM, 2017). Results of the zircon fission track (ZFT) and apatite fission track (AFT) showed multiphase tectono-thermal events developed in the northeastern part of OB. The basin has experienced slow barring and warming in the Triassic to Middle Jurassic. While, the rapid uplift in the early stage of the Early Cretaceous and the Late Cretaceous caused the differential uplift and exhumation (Ding C et al., 2016; Wang JQ et al., 2020). The analysis of oil/gas accumulation demonstrated the peak maturity of source rocks to be in the Late Jurassic and Early Cretaceous (Liu CY and Wu BL, 2016; Chen G et al., 2013). The Early Cretaceous was the key period for the development of intrusions, including the Heshitougou basalt

* Corresponding author: *E-mail address*: chenyinchain@sina.com (Yin Chen); jianguo_lee@126.com (Jian-guo Li).

Literary editor: Li-qiong Jia
doi:10.31035/cg20230068
2096-5192/© 2025 China Geology Editorial Office.

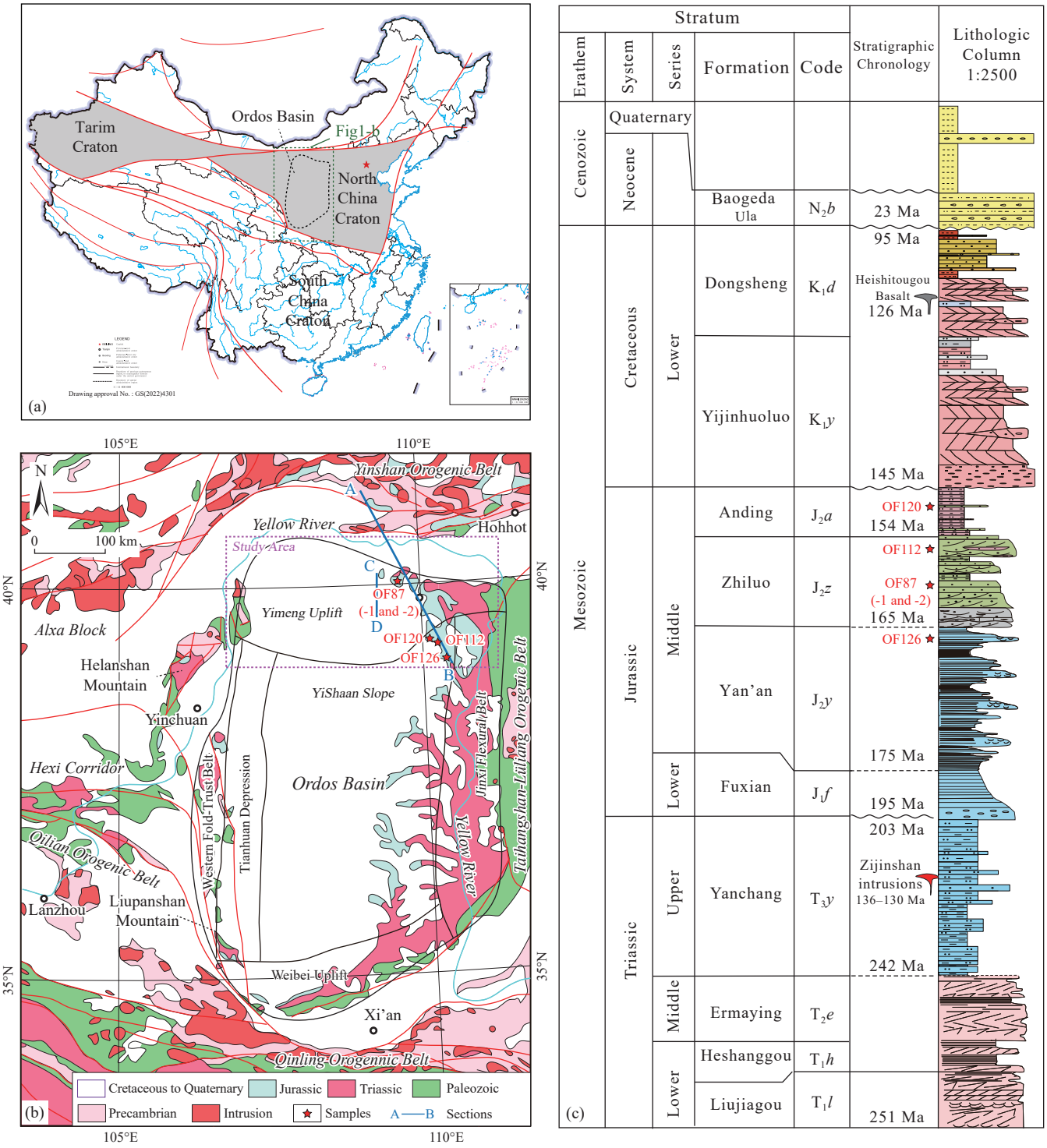

Fig. 1. Regional location (a), geological map of the Ordos Basin (b), and the Mesozoic-Cenozoic stratigraphic column (c). A–B and C–D are the locations of the profiles in Fig. 2. The red pentagrams are the locations of samples. The ages of Zijinshan intrusions from Chen G et al., 2012, and the ages of Heshitougou basalt are from Zou HP et al., 2008.

in the northern part and the Zijinshan intrusion in the eastern part (Ren ZL et al., 2020 and references therein). Three tectonic sequences in the Mesozoic were recognized based on the analyses of the Hangjinqi faults zone (Yang MH et al., 2013, 2015). Based on the observation and analysis of paleo-stress, Zhang YQ et al. (2006, 2011) have pointed out the Late Mesozoic transition of compression and extension in the OB and discussed the stress directions.

However, most of the above achievements were concentrated on the evolution in the Late Mesozoic, especially after the Jurassic. Only a few papers have stated the convincing chronological data for the Early Mesozoic tectonic evolution of the basin and the surrounding orogenic belts. Besides, different research methods would record the difference in the spatial-temporal distribution of the basin uplift and denudation. As for the large-scale sedimentary

basin, its long-time tectonic reworking and denudation would record the significant tectonic events of the basin evolution and the regional tectonic transformation (Liu CY and Wu BL, 2016). With the combined effect of the closure of the Paleo-Asian Ocean, Tethys tectonic movements, and the subduction of the Paleo-Pacific Ocean, it is recognized that the OB has experienced muti-cycle evolution (Zhang YQ et al., 2011; Liu CY and Wu BL, 2016). However, the detailed dynamic mechanism and time of the tectonic events are still debated.

Generally, the low-temperature chronological dating can provide different constraints on the thermal history of the sedimentary basins or orogenic belts (Reiners PW, 2009; Zhou ZY, 2014; Chew D and Spikings R, 2015; Malusà GM and Fitzgerald GP, 2019). These chronological studies have been widely used to explore and discuss the tectonic evolution of the OB and its surroundings (Ehlers TA and Farley KA, 2003; Reiners PW et al., 2002, 2005; Zheng DW et al., 2006; Chen G et al., 2007; van Soest MC et al., 2011; Ren ZL et al., 2015; Chen Y et al., 2022; Tang XY et al., 2022), such as the ZFT, AFT, zircon (U-Th)/He dating (ZHe) and apatite (U-Th)/He dating (AHe). Especially, the apatite and zircon Helium dating is widely applied to track the thermochronology of basins, exhumation of rocks, and orogenic evolution (Reiners PW, 2005; Cooper FJ et al., 2011; Coble MA et al., 2017; Colleps C et al., 2018). (U-Th)/He isotopic systems have relatively low closure temperatures, 40–85°C for apatite (Helium Partial Retention Zone, PRZ) (Warnock AC et al., 1997; Wolf RA et al., 1998; Flowers RM et al. 2009; Gautheron C et al. 2009) and 130–210°C for zircon (Guenthner WR et al. 2013), compared to the other major methods of thermochronology. They can record many youngest tectonic events to build a systemic evolution together with other chronological methods.

In this study, the ZHe and AHe analyses were performed and provided important chronological data to track the tectono-thermal evolution of the northern part of OB and the YOB. Furthermore, the chronological data of the ZFT, AFT, and $^{40}Ar/^{39}Ar$, were collected and analyzed. The Mesozoic evolution and regional motivation mechanism of the basin and its surroundings are systematically discussed, which is crucial for further recognizing the basin evolution in the Mesozoic.

2. Geological setting

The Ordos Basin is located at the western part of the North China Craton, and is separated from the eastern part by the TLOB (Fig. 1). The basin is regarded to be located in the transitional zone between eastern China and western China. There are six subunits including the Yimeng Uplift, Western Fold-Fault Belt, Tianhuan Depression, Yishaan Slope, Jinxi Flexural Belt, and Weibei Uplift in the OB (Fig. 1b).

The basin developed on the Archean and Lower Proterozoic metamorphic basement and experienced multiple evolutionary phases from Paleozoic marine sedimentation to Mesozoic continental sedimentation to Cenozoic fault-depression activity (Liu CY et al., 2006; Jiang L et al., 2016). Since the Mesozoic, the sedimentation and tectonic evolution of the OB have led to the formation of Triassic hydrocarbon sources, Jurassic coal seams and uranium-bearing beds, and a Cretaceous aeolian sedimentation system (Liu CY and Wu BL, 2016; Miao PS et al., 2020; Chen Y et al., 2022). While a series of regional unconformities were developed in the Mesozoic successions (Fig. 1c).

The northern part of OB was separated from the provenance of the YOB by the Cenozoic Hetao rift basin (Figs. 1, 2). Since the Late Cretaceous, the northern part of OB was in uplifted and suffered denudation (Liu CY et al., 2006; Zhao JF et al., 2020). Influenced by the tilted movement, the Triassic Yanchang formation, the Jurassic Yan'an and Zhiluo formations, the Cretaceous Yijinhuoluo and Dongsheng formations of Zhidan Group were exposed to the surface and exhibited as an arc in the northeastern part of OB (Figs. 1b, 2, 3). The NEE-trend Boerjianghaizi fault has cut across the Cretaceous succession and its underlying layers (Fig. 2; Yang MH et al., 2015). The Heishitougou basalt intruded into the Lower Cretaceous Dongsheng Formation with a $^{40}Ar/^{39}Ar$ dating of 126 Ma (Zou HP et al., 2008). In the eastern margin, the Zijinshan intrusions developed in the Triassic successions and have the age of 136–130 Ma (Chen G et al., 2012). The oil/gas, coal, and sandstone-type uranium deposits were preserved in the Late Paleozoic and Mesozoic depositions (Liu CY and Wu BL, 2016).

3. Sampling and methods

Five samples were collected from the sandstone of the Jurassic Yan'an, Zhiluo, and Anding formations in the northern part of OB (Fig. 1b; Table 1). OF120 is the gray-green siltstone from the Middle Jurassic Anding Formation. OF87-1 and OF87-2 are the yellow calcareous medium sandstones from the channel sand-body of the Middle Jurassic Zhiluo Formation. OF112 is the yellow-green medium sandstone from the top layer of the Middle Jurassic Zhiluo Formation. OF126 is the gray medium-fine sandstone from the Yan'an Formation (Fig. 1c). All apatite and zircon grains were separated using standard crushing, sieving, and magnetic and heavy liquid separation methods by the Yu-Neng Technology Service Limited Company, Langfang, Hebei, China. First, apatite and zircon were separated by using standard density and magnetic separation techniques, and then the grains with no inclusions and fractures were hand-picked under a binocular microscope. The widths of the crystals are generally between 68.3–154.6 μm (Fig. 4a).

The (U-Th)/He analyses were performed at the Isotope Thermochronology Laboratory, Chinese Academy of Geological Sciences. Based on the purity, brightness and morphology, the grains were hand-picked and wrapped up in Platinum or Niobium capsules. The measure data of length and width were calculated with alpha ejection correction (F_T; Farley KA, 2002). The length and width were measured for alpha ejection correction. The extraction and analysis of He were carried out by the mass spectrograph of Alphachron Ⅱ

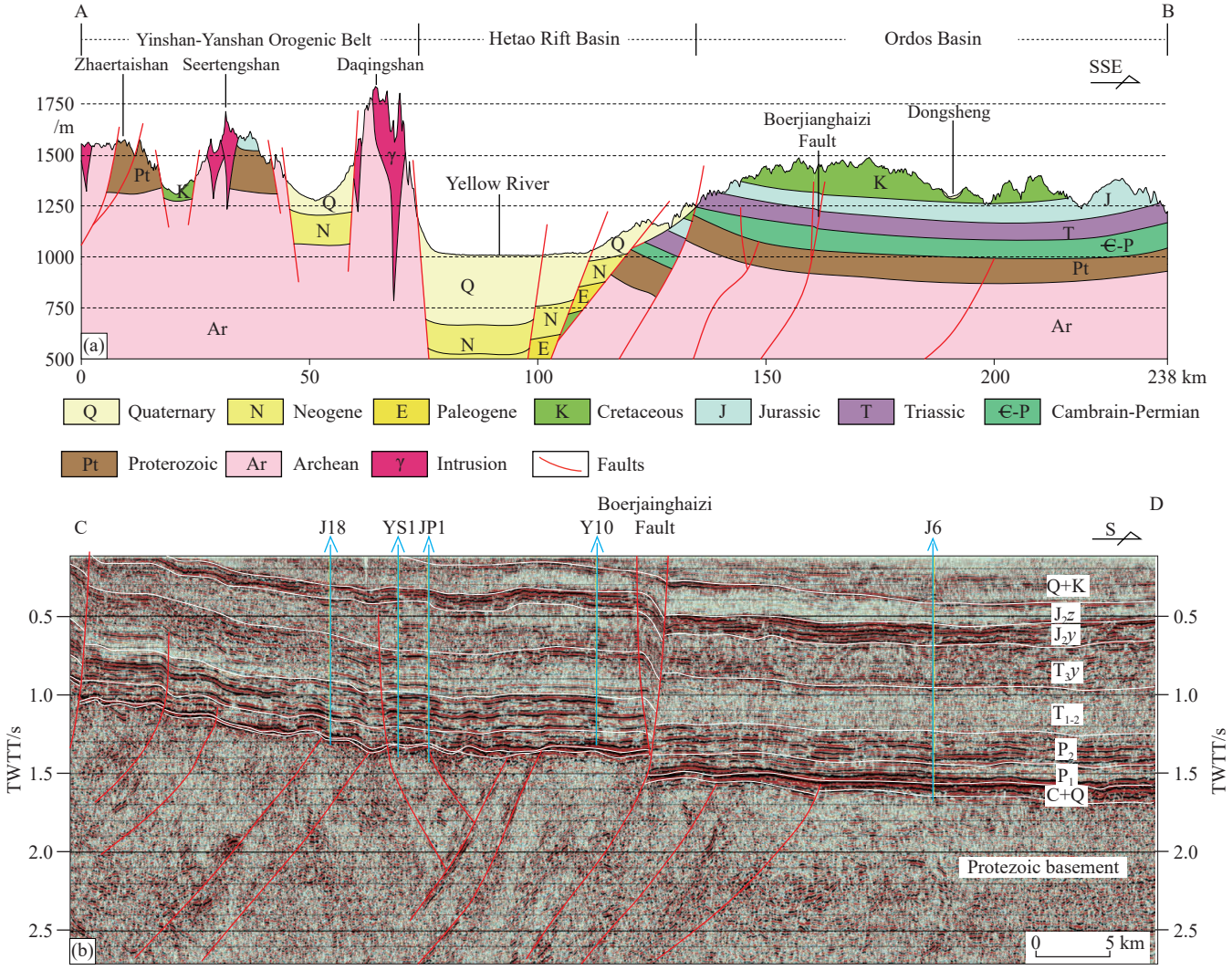

Fig. 2. Geological profile of the northern part of the OB and the YOB (a) and the seismic profile of the Boerjianghaizi fault in the northern part of the OB (b) (the seismic section was modified from Yang MH et al., 2013).

(1300°C for zircon, 900°C for apatite). The values of $^4He/^3He$ were determined by the Quadrupole Mass Spectrometer and standardized by the ^4He standard gas. The apatite and zircon grains were dissolved, and U and Th were measured by the ICP-MS. The standard sample for zircon and apatite was the Sri Lanka zircon [(U-Th)/He dating of 479.0 ± 8.0 Ma] and Durango apatite [(U-Th)/He dating of 31.5±1.4 Ma] respectively. The detailed measured processes for zircon and apatite (U-Th)/He were according to Sun JB et al., 2015, 2017. Five crystals from each sample were analyzed in this work (Table 1).

For the (U-Th) /He dating, results are recognized to be influenced by some factors, such as the U and Th concentration difference, banding in the single crystal, size, and structure difference of crystal, inclusion, α calibration, and so on. Commonly, the dispersion of dating data caused by the differences among crystals is much larger than the one caused by the testing precision (Boyce JW and Hodges KV, 2005; Reiners PW and Nicolescu S, 2006). The dispersion of ages was also affected by the geological process. The effective uranium content (eU, U + 0.235 × Th, in 10^{-6}) and cooling rate may be regarded as the major factors (Guenthner WR et al., 2011, 2013), which even cause the dating data of the ZHe and AHe are larger than the results of the fission track analysis (Green PF and Duddy IR, 2006; Shuster DL et al., 2006). eU would reflect the radiation damage and its effects on the (U-Th) /He dating data or the detailed thermal histories (Flowers RM et al., 2009; Shuster DL et al., 2006).

The high value of U, Th contents in the sample or associated minerals would result in the generation and accumulation of ^4He. The implantation of ^4He in the crystal could cause the age to be older (Spiegel C et al., 2009; Gautheron C et al., 2013; Murray KE et al., 2014). The effect of α implantation is remarkable as eU＜5 μg /g, which can also be indicated by the negative correlation between eU and (U-Th) /He ages (Spiegel C et al., 2009). In this situation, the 20 μm coating of crystal should be removed to make the α-ejection correction. Guenthner WR et al. (2011, 2013) also pointed out that the positive or negative correlation between eU and (U-Th) /He ages may exist due to the differences in thermal histories and degrees of radiation damage.

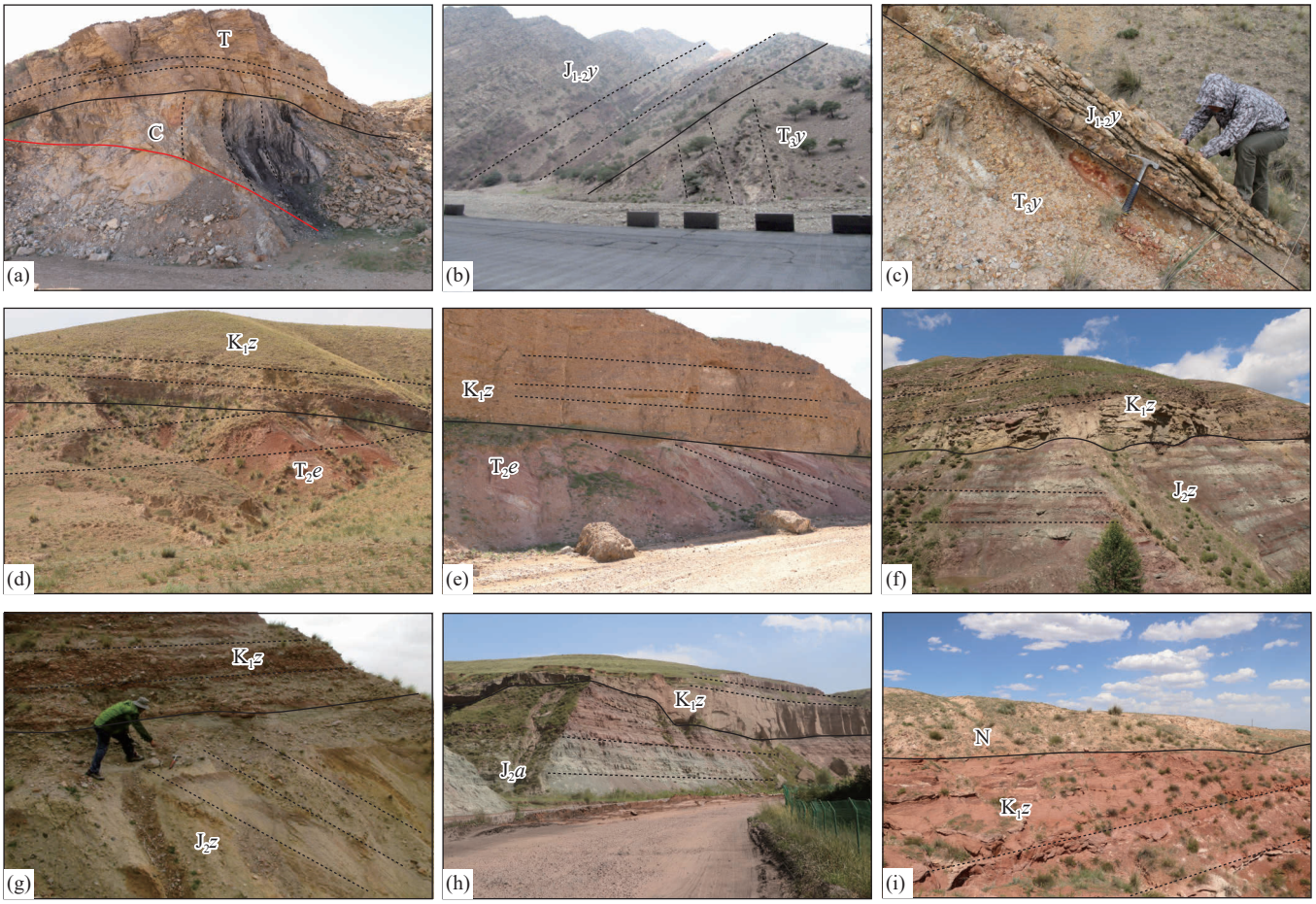

Fig. 3. Geological unconformities among the successions in the northern part of OB. a–Unconformity between the Carboniferous (C) and Triassic (T) in the northeast of the Dongsheng, Inner Mongolia; b–unconformity between the Triassic Yanchang Formation (T_3y) and Jurassic Yan'an Formation ($J_{1-2}y$) in the northeast of the Dongsheng; c–unconformity between the Triassic Yanchang Formation (T_3y) and Jurassic Yan'an Formation ($J_{1-2}y$) and the paleo crust of weathering in the northeast of the Dongsheng; d, e–unconformity between the Triassic Ermaying Formation (T_2e) and the Cretaceous Zhidan Group (K_1z) in the northeast of the Dongsheng; f, g–unconformity between the Jurassic Zhiluo Formation (J_2z) and the Cretaceous Zhidan Group (K_1z) in the northeast of the Dongsheng; h–unconformity between the Jurassic Anding Formation (J_2a) and the Cretaceous Zhidan Group (K_1z) in the northeast of the Yuling, Shaanxi; i–unconformity between the Lower Cretaceous Zhidan Group (K_1z) and the Neogene (N) in the north of the Dongsheng.

4. Results and interpretation

The results of the zircon and apatite (U-Th)/He analyses are given in Table 1.

In this work, the zircon and apatite grains with a spherical radius >70 μm and less of fluid inclusions were chosen. It would improve correction accuracy and reduce the effect of α-ejection correction and the ^{4}He diffusion (Vermeesch P et al., 2012). There is no apparent correlation between (U-Th)/He ages and other possible criteria, such as crystal size, or eU content (Fig. 4). The data set includes crystals with a wide range of sizes (equivalent sphere radius between 37.9 μm and 106.8 μm) and eU contents (ranging from 6.74×10^{-6}–502.34×10^{-6}) (Table 1). This further indicates that the effect of α implantation can be ignored, and the samples have experienced rapid cooling histories (Guenthner WR et al., 2014).

The ZHe dating ages ranged from 419–174 Ma with the spreading summit in the Middle Triassic. The measured ZHe ages are all older than the depositional age of the sampled units (Table. 1), supporting that ZHe system has not been reset after Late Jurassic. The ZHe system of samples has recorded tectono-thermal histories of the provenance. Among them, OF87-1 has a weighted average age of 243±8 Ma (3 grains) with the youngest age of 185 Ma. OF112 have a weighted average age of 235±21 Ma (4 grains). OF120 have a weighted average age of 236±24 Ma (5 grains). OF126 has a weighted average age of 240±65 Ma (3 grains) with the youngest record of 174 Ma. All samples exhibit a similar age distribution pattern, which further states they have the same provenance.

While the AHe data of OF87-2 have an age ranging from 195 Ma to 131 Ma with a weighted average age of 141±22 Ma (3 grains). The AHe mean age was younger than the depositional age and supported that AHe system has not been reset since the Late Cretaceous. Therefore, these data have recorded the tectono-thermal events that lead to the strata uplifting and denudation.

5. Thermal modeling

Inverse modeling of time-temperature (*t*-*T*) histories for

Table 1. AHe and ZHe analysis results of samples from the Jurassic successions in the northern part of the OB.

No.	Sample ID	4He ncc	+/−	Total U/10^{-6}	+/−	Total Th/10^{-6}	+/−	Th/U	FT factor	Mass/ μg	Uncor. Age/ Ma	FT Cor. age/ Ma	+/− Ma	Sphere radius/ μm	Weighted average Age/Ma	+/−/ Ma
1	OF87-1-1 Zr	9.076	0.227	55.167	2.0675	36.3423	1.4285	0.68	0.781	5.9	197.06	252.45	8.08	58.9	243	8
	OF87-1-2 Zr	14.4618	0.3616	288.3944	10.8145	175.7364	6.9007	0.63	0.688	2.2	163.49	237.7	6.72	41.3		
	OF87-1-4 Zr	12.6711	0.3168	142.3994	5.3311	45.843	1.8078	0.33	0.745	3.7	180.62	242.37	7.69	50.1		
	OF87-1-3 Zr	53.0918	1.3274	459.5935	17.1803	181.8793	7.3096	0.41	0.783	5.9	145.13	185.27	6.09	59.1		
	OF87-1-5 Zr	17.9463	0.4487	87.0791	3.2625	84.3196	3.3291	0.99	0.749	4.3	314.24	419.77	12.67	51.8		
2	OF87-2-1 AP	7.0203	0.1767	7.7751	0.1794	36.4222	0.7937	4.81	0.872	23.58	148.8	170.72	4.44	106.8		
	OF87-2-2 Ap	1.7539	0.0439	8.6688	0.2047	9.0302	0.2025	1.07	0.827	8.18	161.98	195.75	5.13	75.7		
	OF87-2-3 Ap	3.0245	0.0757	29.425	0.681	4.2742	0.097	0.15	0.82	6.94	117.22	142.94	3.91	70.4	141	22
	OF87-2-4 Ap	0.3536	0.0089	5.2079	0.1273	6.5084	0.1514	1.28	0.768	3.76	114.41	148.94	3.64	56.6		
	OF87-2-5 Ap	0.4133	0.0104	6.1421	0.1474	3.8672	0.0904	0.65	0.788	4.63	103.86	131.86	3.4	60.8		
3	OF112-1 Zr	28.4613	0.7116	60.7369	2.2705	78.5349	3.0769	1.33	0.805	9	321.94	400.08	12.67	67.3		
	OF112-2 Zr	35.4048	0.8852	150.5019	5.6266	51.9941	2.0441	0.35	0.816	9.1	193.51	237.15	8.22	69.4	235	21
	OF112-3 Zr	79.1524	1.9789	342.7607	12.8471	230.1827	9.2378	0.69	0.766	8.6	189	246.87	7.74	55.1		
	OF112-4 Zr	70.7688	1.7693	240.0379	8.974	140.5338	5.5596	0.6	0.802	12.1	175.06	218.26	7.21	65.1		
	OF112-5 Zr	188.1795	4.7045	489.8613	18.326	372.3527	14.5507	0.78	0.806	13.6	194.47	241.23	7.89	66.8		
4	OF120-1 Zr	2.4991	0.0625	37.5213	1.4077	35.1803	1.392	0.96	0.709	2.6	169.76	239.51	6.78	44.7	236	24
	OF120-2 Zr	14.1709	0.3543	322.3382	12.0566	115.4539	4.5295	0.37	0.674	2	166.3	246.88	7.03	39.2		
	OF120-3 Zr	14.0932	0.3524	212.812	7.9767	82.6549	3.2476	0.4	0.72	2.8	179.34	249.03	7.57	45.7		
	OF120-4Zr	21.7972	0.545	416.5267	15.6242	208.4631	8.2195	0.51	0.684	2.6	148.45	216.95	6.17	40.7		
	OF120-5 Zr	20.2891	0.5073	296.1808	11.0786	86.854	3.4941	0.3	0.7	2.2	237.42	339.19	10.2	42.5		
5	OF126-1 Zr	8.6293	0.2158	190.4437	7.1279	129.6713	5.0795	0.7	0.706	2.6	122.99	174.18	5	44		
	OF126-2 Zr	9.3808	0.2346	199.2274	7.4587	88.6545	3.5066	0.46	0.684	2.4	147.39	215.41	6.16	40.6	240	65
	OF126-3 Zr	8.8146	0.2204	235.4956	8.8724	113.8394	4.498	0.5	0.661	1.7	165.89	250.93	6.94	37.9		
	OF126-5 Zr	12.4068	0.3102	277.7824	10.4128	118.8724	4.6795	0.44	0.681	1.8	180.91	265.57	7.61	40.2		
	OF126-4 Zr	0.0326	0.0009	357.0466	13.3535	148.3217	5.8107	0.43	0.681	1.8	0.38	0.56	0.02	40.2		

Note: The weighted average ages were calculated by the bolded black data in the list of FT Cor. Ages.

(U-Th)/He datasets is common to recover the tectono-thermal evolution and hydrothermal reheating. The HeFty 2.0.0 software package was used to model this thermal history of the zircon and apatite grains based on the (U–Th)/He datasets (Ketcham RA, 2005). Besides, the authors adopt the diffusion model of Guenthner WR et al. (2013) for ZHe, and Farley KA (2000) for AHe. The Monte Carlo statistical approach was employed to test numerous random *t-T* paths that go through the constraint condition. The constraint conditions were chosen according to the regional tectonic evolution stages, deposition and burial history, and key thermal events (Fig. 5). The constraint conditions were as follows: (1) As the samples from the Jurassic successions ought to be exposed to the surface as the sources before or in the Jurassic, the

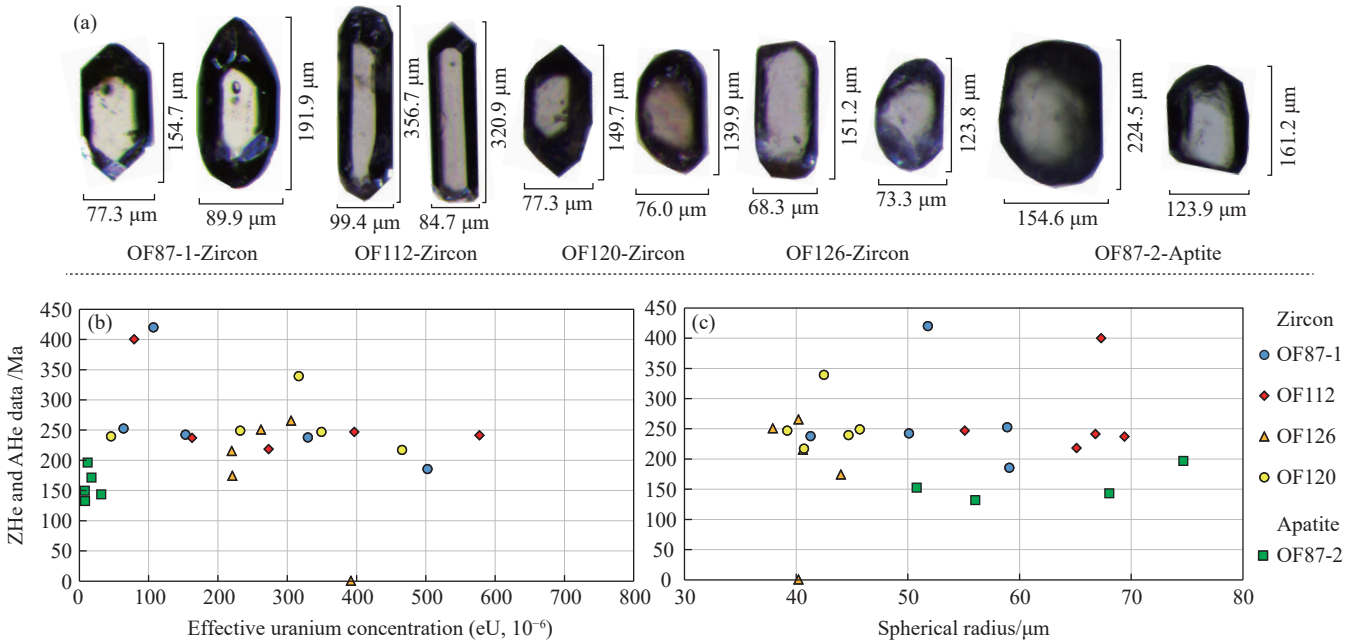

Fig. 4. Microscope photos of zircon and apatite selected for the (U-Th)/He dating (a), plots of corrected ZHe and AHe age versus effective uranium content (eU) (b) and equivalent sphere radius (SR) (c).

temperature was limited to the scale of 0–40°C. (2) According to the paleo-geotemperature recovery in Fig. 6 and the huge thick deposition in the Cretaceous, the scale of temperature from the Late Jurassic to Early Cretaceous was chosen from 0°C to 120°C. (3) Since the Late Cretaceous, the OB was suffered from denudation with a little amount of Neocene deposition, and the scale of temperature from the Late Jurassic to Early Cretaceous was restricted from 0°C to 60°C. (4) The paleo- and present mean surface temperature is assumed to be 20°C. (5) The starting time of the thermal history is selected as the maximum age recorded by the crystals. In the modeling, the goodness-of-fit (GOF) parameter was used to assess the fitness between the modeled results and the analyzed data. The results were interpreted to be acceptable when GOF was ⩾0.05 and good when GOF was ⩾0.5 (Ketcham RA, 2005). For all samples, inverse thermal history modeling was run for 10000 paths. Over 100 good random time-temperature (*t-T*) paths were used to ensure that the modeling was adequate.

The modeling results are shown in Fig. 5. Most of the samples experienced a high initial temperature and rapid cooling rate during the Late Permian to Early Triassic (ca. 290–245 Ma). Especially, the pattern of OF112 has been exposed to the surface and kept a flat pattern until the Early Jurassic. Influenced by the tectono-thermal events in the Late Triassic to Early Jurassic, other samples were brought to the surface as the source for the Jurassic deposition. Then all samples were buried again with the huge thickness of Jurassic and Early Cretaceous depositions. However the patterns of OF87-1 and OF126 have recorded rapid cooling during the Late Jurassic and Early Cretaceous. Meanwhile, the highest temperature would be up to ca. 100°C. Except for OF87-1, the thermal patterns showed rapid cooling from the Late Cretaceous to the Early Paleocene. Besides, the thermal histories of OF120 and OF126 also recorded the cooling in the Miocene, which is not discussed in detail in this work.

6. Discussion

In the Mesozoic, the OB experienced complex and episodic tectonic activities. Based on the analyses of thermal evolution histories and paleo-geotemperature recovery, the maximum buried depth of the Middle Jurassic Yan'an, Zhiluo, and Anding Formations in the northern part of OB were estimated to be up to ca. 1400–1800 m (Fig. 6). According to the paleo-geothermal gradient, the highest paleo-temperature would be 105–120°C (Fig. 6). Therefore, the samples from the above formations have crossed the closure temperature of AHe system, which recorded the thermal evolution of the basin. On the other side, they still did not cross the closure temperature of the ZHe system, which has recorded the thermal events of the provenance.

To further understand the Mesozoic tectono-thermal evolution of the northern part of OB and its surroundings, and discuss the regional dynamic background, a series of thermal chronological data were also collected and analyzed in this work. Fig. 7 shows the location of these data including AFT, ZFT, and $^{40}Ar/^{39}Ar$. The contrastive analysis has been conducted on the tectono-thermal evolution of the northern part of OB, the western part of OB, the Helanshan orogenic belt, the YOB, and the TLOB (Fig. 8). The *t-T* patterns of the northern part of OB and the YOB have been built up. The analysis data modeling results of this study, and other geochronological data indicate that the northern part of OB and the YOB have experienced the four stages of tectono-thermal evolution in the Mesozoic.

6.1. Late Permian-Early Triassic

In the northern part of OB, ZHe dating ages from 4

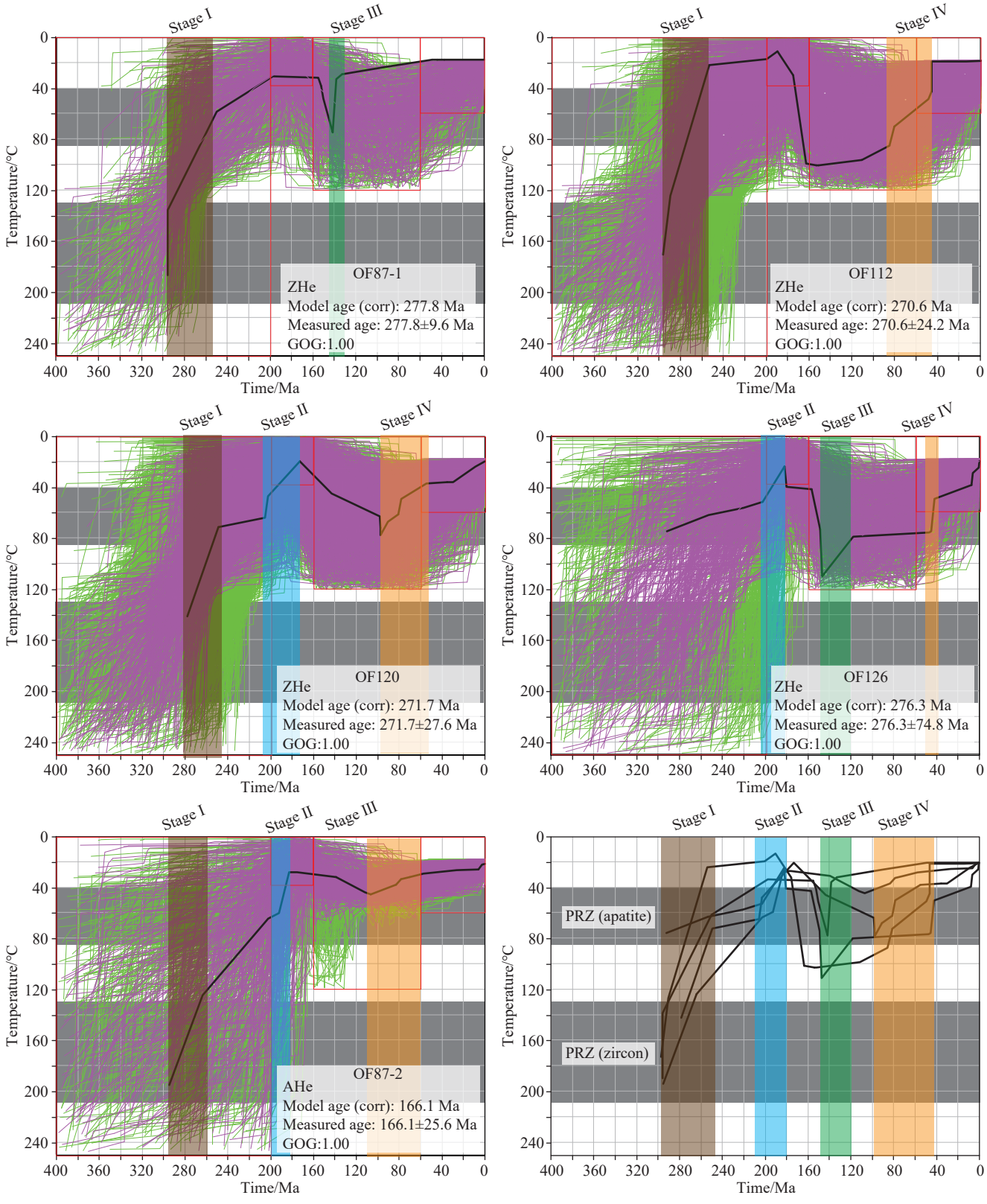

Fig. 5. Thermal history modeling results by using HeFTy. The purple and green curves represent the "good" and "acceptable" paths, and the bold black curves represent the best-fit paths. AHe partial retention zone (PRZ) ranges from 40°C to 85°C; while ZHe PRZ from 130°C to 210°C. The red boxes are the constraint conditions for thermal modeling.

samples in the Jurassic Yan'an and Zhiluo Formation ranged from 243 Ma to 229 Ma, which were older than the depositional age (Table 1). The paleogeothermal gradient in Fig. 6 indicated that all zircon grains did not experience the cooling after deposition, and were regarded to still record the thermal histories of the provenance. The thermal modeling showed that all samples had experienced the rapid cooling event during ca. 290–240 Ma. The intensive tectonic uplifting

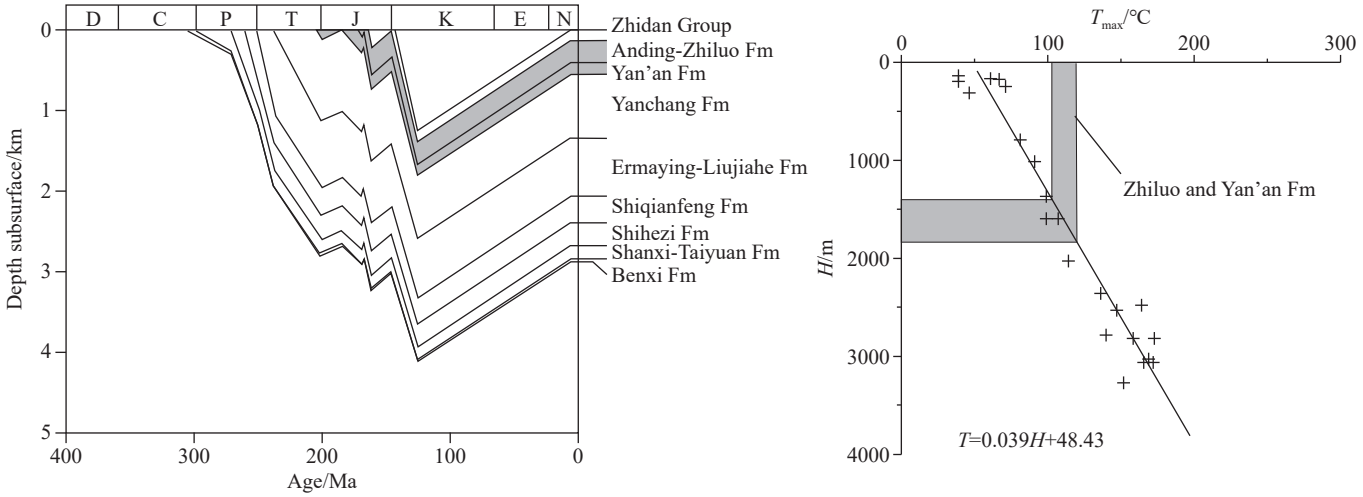

Fig. 6. Simulated thermal evolution history in the northern part of OB (left; modified from Ren ZL et al., 2006) and the highest paleo-temperature *vs*. depth in the Yimeng uplift (right; modified from Yu Q and Ren ZL, 2008).

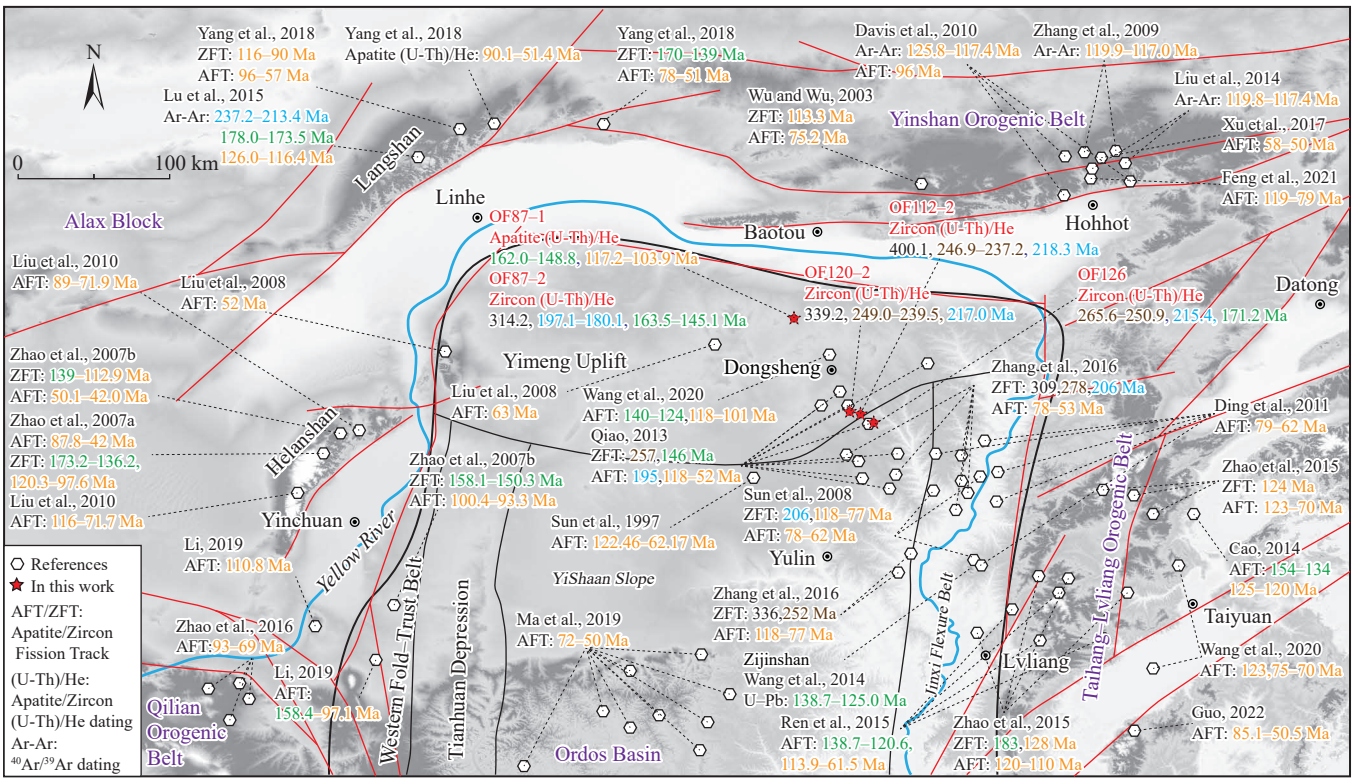

Fig. 7. Thermal chronological data in the northern part of OB and its surroundings. Colors of the ages represent different stages of the tectonic evolution. The brown color is for the period of Late Permian-Early Triassic. The blue color is for the period of the Late Triassic-Early Jurassic. The green color is for the period of the Late Jurassic-Early Cretaceous. The orange color is for the period of the Late Cretaceous-Early Paleogene (Wu ZH, 2003; Liu WS et al., 2008; Sun JB, 2008; Zhang JJ et al., 2009; Ding C, 2010; Davis GA and Darby BJ, 2010; Liu JH et al., 2010; Guo L et al., 2012; Qiao JX, 2013; Cao XZ, 2014; Liu J et al., 2014; Lu YP et al., 2015; Ren XM et al., 2015; Huang ZG et al., 2016; Zhang WL, 2016; Zhao XC et al., 2016; Xu QQ et al., 2017; Yang XC, 2018; Li B, 2019; Ma XJ et al., 2019; Wang JQ et al., 2020; Feng LX et al., 2021; Guo XQ, 2022).

of the YOB in the Late Permian-Early Triassic was indicated by the analysis of ZHe and AHe from the deposition in the OB.

The samples from the deposition may record the geochoronological data of the units in the provenances (Dickinson WR and Gehrels GE, 2009; Thomas WA, 2011). The chronological data of detrital zircons from the Jurassic and Cretaceous successions were collected, combined with the ages of the intrusions in the YOB (Fig. 9). Figs. 8 and 9 show that the tectono-thermal event recorded by the ZHe system acted at ca. 244 Ma which was younger than the intruding ages of the intrusions in the YOB at ca. 268 Ma. Besides, the major mineralization ages in the YOB were also consistent with the activities of the thermal events and

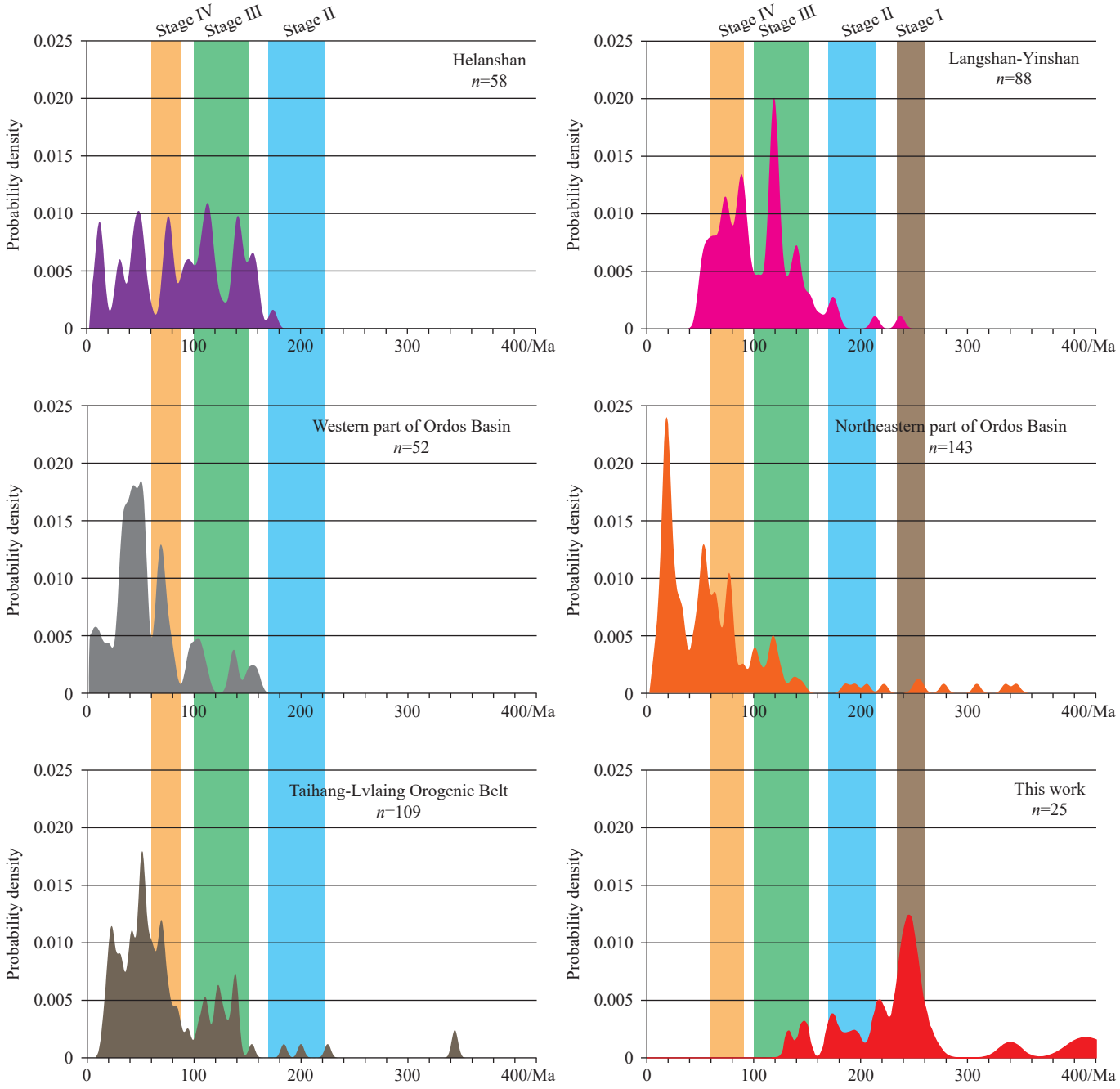

Fig. 8. Probability of chronological data in the northern part of OB and its surroundings (please see the references in Fig. 7 for the data sources).

intrusion (Fig. 9). The *t-T* cooling paths in Fig. 10 also suggested the first rapid cooling event start during the Late Permian-Early Triassic. These data have recorded the closure of the Paleo-Asian Ocean with the massive magmatic events and mineralization. The regional unconformity developed between the Triassic and Carboniferous (Fig. 3a) also presented this tectonic uplift in the northern part of OB.

The Late Permian-Early Triassic is the significant development stage of the Central Asian Orogenic Belt (CAOB) (Xiao WJ et al., 2015; Imayama T et al., 2019; Zhang C et al., 2020; Wang B and Zhao GC, 2021; Dang ZC et al., 2022; Wang T et al., 2022; Ma YF et al., 2022). The subduction and collision between the Siberia Plate and the NCC caused the closure of the Paleo-Asian Ocean. The E-W trending magmatic belt spread along the northern margin of the NCC in the period of the Late Paleozoic to Early Mesozoic, especially Triassic sodic granites of 246–236 Ma responding to the collision, extrusion and thicken (Li S et al., 2016; Wu D et al., 2021). The regional tectonic regime of the OB and the YOB transferred from back-arc extension to collision and extrusion, which drove the exposition of the YOB and uplift of the Yimeng Uplift in the OB to be the new provenances for the basin (Chen AQ et al., 2011; Chen QH et al., 2012). Meanwhile, the marine depositional system in the basin transferred to the continental depression sedimentary system (Li JY, 2009; Zhang XH and Zhai MG, 2010; Zhao Y

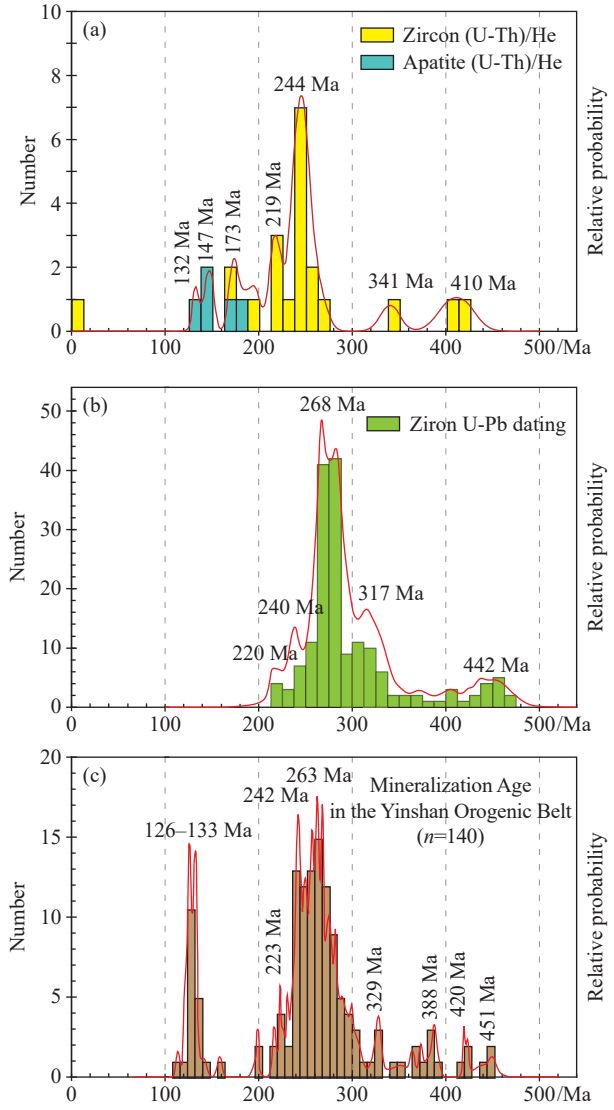

Fig. 9. Geochronological data distribution patterns in the northern part of OB and the YOB. a–the AHe and ZHe data in this work; b–detrital zircon U-Pb data from the Jurassic Zhiluo formation and Zhidan Group (Stevens T et al., 2013; Chen Y et al., 2017) and intrusion Zircon U-Pb data from the YOB (Guo L et al., 2012); c–mineralization age in the YOB (Zhang HT et al.,1999; Nie FJ et al., 2002, 2005; Liu YF et al., 2011; Zhang YM et al., 2011; Zhang RR, 2015; Li ZD et al., 2020; Wu HH et al., 2020; Zhang HD et al., 2021, and references therein).

et al., 2017).

As a result, the tectonic evolution of the northern margin of the NCC in the Late Permian-Early Triassic was characteristic of the subduction and collision (Fig. 11a). Until the closure of the paleo-Asian Ocean and development of the Mongol-Okhotsk Ocean, compressional uplifts and thrusts were widely developed along the YOB as the significant sources for the deposition of the Mesozoic successions.

6.2. Late Triassic-Early Jurassic

The geochronological data of 218–171 Ma were recorded in many grains (Table 1) and the thermal patterns (Fig. 5). It stated that the YOB experienced continued cooling and uplifting to be the major provenance. Unconformities commonly developed above the Triassic Ermaying Formation and Yanchang Formation. The paleo-weathering crust was found in the Yanchang Formation and covered by the Middle Jurassic Yan'an Formation (Figs. 3b–c). The chronological data distributions in Figs. 8 and 9 stated that the Late Triassic was the secondary peak age for the uplifting in the northern part of OB and YOB. Fig. 10 shows the rapid cooling rate of the YOB and OB in the Late Triassic-Early Jurassic.

During the Early-Middle Triassic, the northern part of OB and the YOB were in the regime of post-collisional extension. With the weak regional tectonic activities, the basin was in subsidence and sedimentary (Liu CY et al., 2006). But in the Late Triassic, the continuing collision along the northern margin of the NCC, and the collision tectonics between the NCC and South China Craton (SCC), have reached the peak (Wang T et al., 2009; Wang XX et al., 2015; Zhang XM et al., 2019; Zhang YQ et al., 2019). The movements drove the regional tectonic system from extension to compression. As a result, uplift and thrust widely spread in the YOB with the uplift of the eastern part of the NCC (Peng ZM et al., 2009; Yang MH et al., 2012; Liu S et al., 2013).

During 205–190 Ma, the OB has suffered the first large-scale uplift and denudation (Wang JQ et al., 2020). At the end of the Yanchang Formation, the Indosinian movement drove the E-W-direction uplifting and denudation to form the topographical relief in the Early Jurassic. Unconformities laying under the Lower Jurassic succession were commonly discovered in the Yungang-Pinglu basin, OB, Shiguai basin, and Baotou basin (Figs. 1c and 3; Ma YS, 2001; Liu S et al., 2013; Wang Y et al., 2017).

The OB and the YOB have experienced the transition from the post-orogenic extension of the CAOB to the subduction and compression of the Mongol-Okhotsk Ocean in the Late Triassic-Early Jurassic (Fig. 11). Influenced by the collision between the NCC and SCC, the strain state of the OB was in the S-N-direction compression. A series of thrust-nappe structures were developed in the YOB to be the major source area. Although the arguments about the start time of the subduction of the Paleo-Pacific Ocean still existed, it was commonly recognized that the subduction would not be later than the Early Jurassic (Xu WL et al., 2013; Wilde SA, 2015; Zhang C et al., 2020) and with the E-W subducting direction (Liu K et al., 2017).

6.3. Late Jurassic-Early Cretaceous

The tectono-thermal events were only recorded by the results of the AHe analysis data in this work (Table 1). The thermal modellings, statistical analysis of dating data have recorded this rapid cooling event (Figs. 5, 6, 7, and 8). The *t-T* patterns of Fig. 10 preserve that the OB and the YOB experienced rapid cooling during the Late Jurassic-Early Cretaceous. In the northern part of OB, the Lower Cretaceous Zhidan Group conglomerate was developed, and has an unconformity with the Middle Jurassic Zhiluo and Anding formations (Figs. 3f–h), which indicated the rapid uplift of the

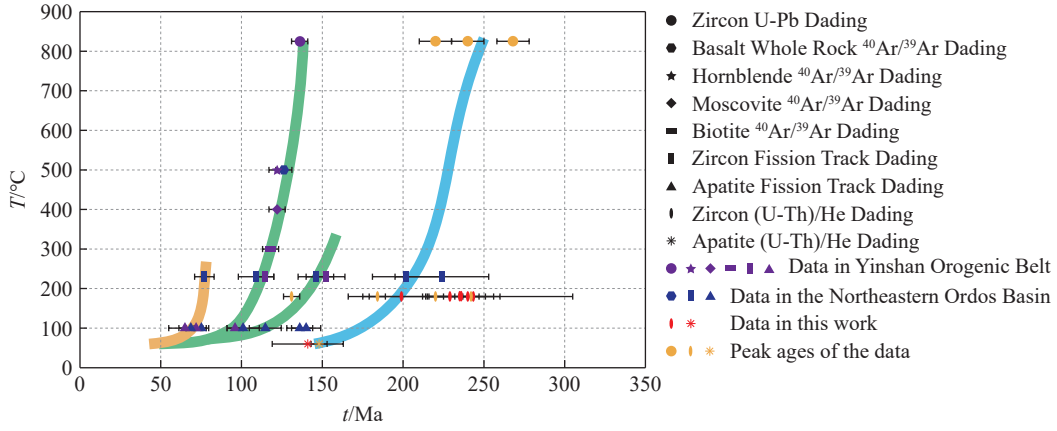

Fig. 10. *t-T* cooling patterns in the northern part of OB and the YOB (see Fig. 7 for the data sources).

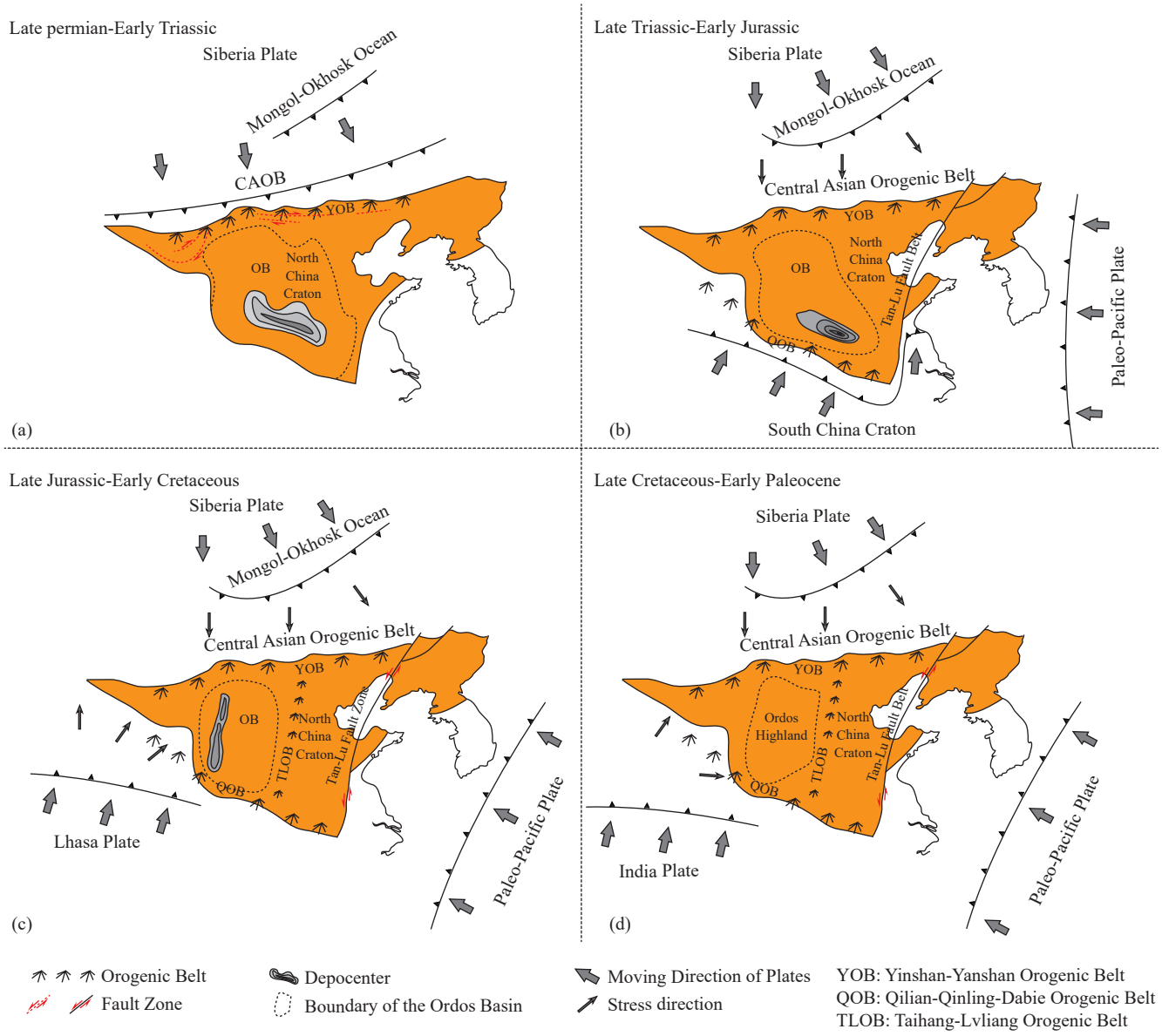

Fig. 11. Regional evolution of the OB and NCC in the Mesozoic and the multi-direction collision.

source area.

During the Late Jurassic–Early Cretaceous, the OB was affected by a tectonic compressive regime with an unconformity (Chen G et al., 2007; Zhao Y et al., 2017). Influenced by the NW-direction high-speed and low-angle subducting of the Paleo-Pacific Plate, the paleogeography of

the NCC underwent a major transformation (Liu YQ et al., 2015; Li SZ et al., 2019; Zhu RX and Xu YG, 2019; Zhang C et al., 2020). The TLOB started to become the highlands and further resulted in the deposition center transferring from the southern to the western part of the basin (Liu CY et al., 2006; Zhao JF et al., 2020). The large-scale thrust-nappe structures developed in the YOB (Zheng YD et al., 1998; Xu ZY et al., 2001; Liu ZH et al., 2003). Accompanied by the closure of the Mongol-Okhotsk Ocean, a series of Late Jurassic–Early Cretaceous plutons spread in the YOB. It was also a significant mineralization period in the YOB (Fig. 9c).

The Late Jurassic–Early Cretaceous is commonly recognized as a significant transitional phase of tectonics in East Asia and is in the background of multi-direction collision (Dong SW et al., 2015; Jiang L et al., 2016). It was also addressed to be the key tectonic event for basin evolution (Chen G et al., 2007). The Mongol-Okhost Ocean closed with the orogenesis in the northern margin of the NCC (Dong SW et al., 2015; Cogné JP et al., 2005; Arzhannikova AV et al., 2020). East Asia began to be dominantly influenced by the subduction of the paleo-Pacific plate (Dong SW et al., 2015; Zhu G et al., 2015), and the Lhasa Block and Indian Plate moved northward toward the Eurasian Plate (Xu ZQ et al., 2006; Song DF et al., 2018). Then, the OB was mainly under the NW-SE direction compressional conditions (Zhang YQ and Liao CZ, 2006; Zhao JF et al., 2020).

6.4. Late Cretaceous- Early Paleogene

This cooling event was exhibited by the thermal evolution paths of samples expect of OF87-1 (Fig. 5). All geochronological data in the OB and its surroundings also have the peak ages in the Late Cretaceous–Early Paleogene (Figs. 7 and 8). The outcrops in the northern part of OB have shown an unconformity between the Lower Cretaceous red sedimentary system and the Neogene calcium cemented sedimentary system (Fig. 3i). Furthermore, the OB was absent of the deposition of the Upper Cretaceous, which also proved the significant tectonic activity to drive the uplift of the basin in the Late Cretaceous (Figs. 1c and 10).

During the Late Cretaceous–Early Paleogene, the OB experienced regional exhumation, with the stress field shifting from extension to compression (Zhang XH and Zhai MG, 2010; Shi W et al., 2006; Ren XM et al., 2015). Since the Late Cretaceous, the East Asian continent began to experience the subductions of the Neo-Tethys Ocean from the southwest and the Paleo-Pacific Ocean from the east (Li JY, 2009; Suo YH et al., 2020). The Indian Plate began to collide with the Eurasian Plate (Jolivet M et al., 2001; Zattin M and Wang X, 2019; Yi ZY et al., 2022). The subduction direction of the Paleo-Pacific plate transferred from NW in the Early Paleogene to NNW after the Neogene (Ge XH et al., 2014; Cheng YH et al., 2018). Influenced by the subduction from the Paleo-Pacific Plate in the east and the collision from the Indian Plate in the southwest, The OB remained in a long-term condition of basin-scale uplifting and exhumation since the Late Cretaceous (Ren ZL et al., 2015; Liu CY and Wu BL, 2016). Some previous works on sandstone-type uranium mineralization also proved that this cooling event controlled their peak metallogenic process in the OB (Wang SY et al., 2020; Chen Y et al., 2022).

7. Conclusions

Based on the tectonic and geochronology analysis of the northern part of the OB, the regional dynamic background in the Mesozoic was further discussed. The results were helpful to understand the tectonic transformation of the NCC and multi-direction collision of plates in the Mesozoic.

The geochronological data of AHe and ZHe analyses from the Jurassic successions in the northern part of OB present to have weighted ages of 240 Ma–235 Ma, and 141 Ma with the peak distribution of 244 Ma, 219 Ma, 173 Ma, 147 Ma–132 Ma.

Combined with the thermal models, the regional unconformities, and the geochronological data of AFT, ZFT, and $^{40}Ar/^{39}Ar$ in the northern part of OB and its surroundings, four stages of regional tectonic evolution for the OB and the YOB were confirmed in the Mesozoic.

In the Late Permian-Early Triassic, The OB and The YOB were major influenced by the closure of the paleo-Asian Ocean and the orogenic process of the CAOB. In the Late Triassic-Early Jurassic, they experienced the transfer from the post-orogenic extension of the CAOB to the subduction and compression of the Mongol-Okhotsk Ocean. Influenced by the collision between the NCC and SCC, the S-N-direction compression caused the uplift and thrust in the OB and YOB. In the Late Jurassic-Early Cretaceous, the closure of the Mongol-Okhost Ocean and subduction of the paleo-Pacific Plate were the major regional tectonic regime. Uplift and orogenic processes widely developed surround the OB and lead to the decrease of the deposition scale. In the Late Cretaceous- Early Paleogene, influenced by the subduction from the Paleo-Pacific Plate and the collision from the Indian Plate, the OB suffered from a long-term basin-scale uplifting and exhumation.

In summary, the multi-direction collision controlled the tectonic evolution of the OB in the Mesozoic. Four stages may reflect the activation or end of different plate movements.

CRediT authorship contribution statement

Yin Chen and Jiang-guo Li conceived of the presented idea and the draft. Lu-lu Chen and Hua-lei Zhao carried out the experiments and draw some figures. All authors discussed the results and contributed to the final manuscript.

Declaration of competing interest

The authors declare no conflicts of interest.

Acknowledgments

This study was jointly supported by the Science &

Technology Fundamental Resources Investigation Program (2022FY101800), National Science Foundation (92162212), the project from the Key Laboratory of Tectonics and Petroleum Resources (China University of Geosciences, Wuhan) (TPR-2022-22), the International Geoscience Programme (IGCP-675). The authors thank the reviewers for their constructive comments and suggestions on the manuscript. We also thank the editorial staff for editing the manuscript.

References

Arzhannikova AV, Demonterova EI, Jolivet M, Arzhannikov SG, Mikheeva EA, Ivanov AV, Khubanov VB, Pavlova LA. 2020. Late Mesozoic topographic evolution of western Transbaikalia: Evidence for rapid geodynamic changes from the Mongol-Okhotsk collision to widespread rifting. Geoscience Frontiers, (5), 1695–1709. doi: 10.1016/j.gsf.2019.12.012.

Boyce JW, Hodges KV. 2005. U and Th zoning in Cerro de Mercado (Durango, Mexico) fluorapatite: Insights regarding the impact of recoil redistribution of radiogenic ^{4}He on (U-Th) /He thermochronology. Chemical Geology, 219(1–4), 261–274. doi: 10.1016/j.chemgeo.2005.02.007.

Cao XZ. 2014. Evolution and Mechanism of Tectonic Geomorphology in The Central North China Block from the Mesozoic to the Cenozoic. Qingdao, Ocean University of China, Master thesis, 52–69 (in Chinese with English abstract).

Chen AQ, Chen HD, Xu SL, Lin LB, Shang JH. 2011. Sedimentary filling of north ordos and their implications for the soft collision process of Hing Gan Mts. -Mongolia Orogenic Belt in Late Paleozoic. Journal of Jilin University (Earth Science Edition), 41(4), 953–965 (in Chinese with English abstract). doi: 10.3969/j.issn.1671-5888.2011.04.001.

Chen G, Ding C, Xu LM, Zhang HN, Li Y. 2012. Analysis on the thermal history and uplift process of Zijinshan intrusive complex in the eastern Ordos basin. Chinese Journal of Geophysics, 55(11), 3731–3741 (in Chinese with English abstract). doi: 10.6038/j.issn.0001-5733.2012.11.020.

Chen G, Li SH, Zhan HR, Ding C, Yang F, Lei PP. 2013. Timing and stages of the Permian oil-gas accumulations in northeastern Ordos Basin. Geology in China, 40(5), 1453–1465 (in Chinese with English abstract).

Chen G, Wang ZW, Bai GJ, Sun JB, Zhang HR, Li XD. 2007. Meso-Cenozoic peak-age events and their tectono-sedimentary response in the Ordos Basin. Geology in China, 34, 375–383 (in Chinese with English abstract). doi: 10.1631/jzus.2007.B0900.

Chen QH, Li WH, Hu XL, Li KY, Pang JG, Guo YQ. 2012. Tectonic setting and provenance analysis of late Paleozoic sedimentary rocks in the Ordos Basin. Acta Geologica Sinic, 86(7), 1150–1162 (in Chinese with English abstract). doi: 10.3969/j.issn.0001-5717.2012.07.011.

Chen Y, Feng XX, Chen LL, Jin RS, Miao PS, Sima XZ, Miao AS, Tang C, Wang C, Liu ZR. 2017. An analysis of U-Pb dating of detrital zircons and modes of occurrence of uranium minerals in the Zhiluo Formation of northeastern Ordos Basin and their indication to uranium sources. Geology in China, 44(6), 1190–1206 (in Chinese with English abstract). doi: 10.12029/gc20170611.

Chen Y, Miao PS, Li JG, Jin RS, Zhao HL, Chen LL, Wang C, Yu HY, Zhang XR. 2022. Association of sandstone-type uranium mineralization in the northern China with tectonic movements and hydrocarbons. Journal of Earth Science, 33(2), 289–307. doi: 10.1007/s12583-021-1493-0.

Cheng YH, Li Y, Wang S, Li Y, Ao C, Li JG, Sun LX, Li HL, Zhang TF. 2018. Late cretaceous tectono-magmatic event in Songliao basin, NE China, new insights from mafic dyke geochronology and geochemistry analysis. Geological Journal, 53(6), 2991–3008. doi: 10.1002/gj.3137.

Chew D, Spikings R. 2015. Geochronology and thermochronology using apatite: Time and temperature of lower crust to surface. Elements, 11, 189–194. doi: 10.2113/gselements.11.3.189.

Coble MA, Burgess SD, Klemetti EW. 2017. New zircon (U-Th)/He and U/Pb eruption age for the Rockland tephra, western USA. Quaternary Science Reviews, 172, 109–117. doi: 10.1016/j.quascirev.2017.08.004.

Cogné JP, Kravchinsky VA, Halim N, Hankard F. 2005. Late Jurassic-Early Cretaceous closure of the Mongol-Okhotsk Ocean demonstrated by new Mesozoic palaeomagnetic results from the Trans-Baikal area (SE Siberia). Geophysical Journal International, 163, 813–832. doi: 10.1111/j.1365-246X.2005.02782.x.

Colleps C, McKenzie NR, Stockli D, Hughes N, Singh B, Webb A, Myrow P, Planavsky, NJ, Horton B. 2018. Zircon (U-Th)/He thermochronometric constraints on Himalayan thrust belt exhumation, bedrock weathering, and Cenozoic seawater chemistry. Geochemistry, Geophysics, Geosystems, 19, 257–271. doi: 10.1002/2017GC007191.

Cooper FJ, van Soest MC, Hodges KV. 2011. Detrital zircon and apatite (U‐Th)/He geochronology of intercalated baked sediments: A new approach to dating young basalt flows. Geochemistry, Geophysics, Geosystems, 12, Q07003. doi: 10.1029/2011GC003650.

Dang ZC, Li JJ, Fu C, Qin GW, Yang BY. 2022. Report of LA-ICP-MS zircon U-Pb dating (272 Ma) of gabbros in Yagan area, northern Alxa, Inner Mongolia: Insights into the tectonic evolution of the southern Paleo-Asian Ocean. China Geology, 5, 188–190. doi: 10.31035/cg2021042.

Davis GA, Darby BJ. 2010. Early Cretaceous overprinting of the Mesozoic Daqing Shan fold-and-thrust belt by the Hohhot metamorphic core complex, Inner Mongolia, China, Geoscience Frontiers, 1, 1–20. doi: 10.1016/j.gsf.2010.08.001

Deng J, Wang QF, Gao BF, Huang DH, Yang LQ, Xu H, Zhou YH. 2005. Evolution of Ordos Basin and its distribution of various energy resources. Geoscience, 19(4), 538–545 (in Chinese with English abstract). doi: 10.1360/gs050303.

Dickinson WR, Gehrels GE. 2009. U-Pb ages of detrital zircons in Jurassic eolian and associated sandstones of the Colorado Plateau: evidence for transcontinental dispersal and intraregional recycling of sediment. Geological Society of America Bulletin, 121, 408–433. doi: 10.1130/B26406.1.

Ding C, Chen G, Guo L, Zhang WL, Liu T. 2016. Differential uplift on the northeast margin of Ordos Basin: Evidence from apatite fission track analysis. Geology in China, 2016,43(4), 1238–1247 (in Chinese with English abstract). doi: 10.12029/gc20160410.

Ding C. 2010. Thermal evolution and petroleum-charging times in the Northeast area of Ordos Basin. Xi'an, Northwestern University, Master thesis, 33–43 (in Chinese with English abstract).

Dong SW, Zhang YQ, Zhang FQ, Cui JJ, Chen XH, Zhang SH, Miao LC, Li JH, Shi W, Li ZH, Huang SQ, Li HL. 2015. Late Jurassic-Early Cretaceous continental convergence and intracontinental orogenesis in East Asia, a synthesis of the Yanshan revolution. Journal of Asian Earth Sciences, 114, 750–770. doi: 10.1016/j.jseaes.2015.08.011.

Ehlers TA, Farley KA. 2003. Apatite (U-Th)/He thermochronometry: Methods and applications to problems in tectonic and surface processes. Earth and Planetary Science Letters, 206(1–2), 1–14. doi: 10.1016/S0012-821X(02)01069-5.

Farley KA. 2000. Helium diffusion from apatite: General behavior as illustrated by Durango fluorapatite. Journal of Geophysical Research, 105(B2), 2903–2914. doi: 10.1029/1999JB900348.

Farley KA. 2002. (U-Th)/He dating: Techniques, calibrations, and applications. Reviews in Mineralogy and Geochemistry 47(1), 819–844. doi: 10.2138/rmg.2002.47.18.

Feng LX, Han BF, Wang ZZ, Kong LJ, Liu B, Zheng B, Ji JQ, Zhang ZC. 2021. Differentialuplift-denudation of the basement in the Daqingshan Mountains, Inner Mongolia, since the Late Mesozoic: constraints from the apatite fission track thermochronology. Acta Geologica Sinica, 95(6), 1727–1742 (in Chinese with English abstract). doi: 10.19762/j.cnki.dizhixuebao.2020271.

Flowers RM, Ketcham RA, Shuster DL, Farley KA. 2009. Apatite (U-Th)/He thermochronometry using a radiation damage accumulation and annealing model. Geochimica et Cosmochimica Acta, 73, 2347–2365. doi: 10.1016/j.gca.2009.01.015.

Gautheron C, Barbarand J, Ketcham RA, Tassan-Got L, van der Beek P, Pagel M, Pinna-Jamme R, Couffignal F, Fialin M. 2013. Chemical influence on α-recoil damage annealing in apatite: Implications for (U-Th)/He dating. Chemical Geology, 351, 257–267. doi: 10.1016/j.chemgeo.2013.05.027.

Gautheron C, Tassan-Got L, Barbarand J, Pagel M. 2009. Effect of alpha damage annealing on apatite (U-Th)/He thermochronology. Chemical Geology, 266, 157–170. doi: 10.1016/j.chemgeo.2009.06.001.

Ge XH, Liu JL, Ren SM, Yuan SH. 2014. The formation and evolution of the Mesozoic-Cenozoic continental tectonics in eastern China. Geology in China, 41, 19–38 (in Chinese with English abstract). doi: 10.3969/j.issn.1000-3657.2014.01.002.

Green PF, Duddy IR. 2006. Interpretation of apatite (U-Th) /He ages and fission track ages from cratons. Earth and Planetary Science Letters, 244(3–4), 541–547. doi: 10.1016/j.epsl.2006.02.024.

Guenthner WR, Reiners PW, Ketcham RA, Nasdala L, Giester G. 2013. Helium diffusion in natural zircon: Radiation damage, anisotropy, and the interpretation of zircon (U-Th)/He thermochronology. American Journal of Science, 313(3), 145–198. doi: 10.2475/03.2013.01.

Guenthner WR, Reiners PW, Ketcham RA, Nasdala L. 2011. Development of a radiation damage and annealing model for the zircon (U-Th)/He Thermochronometer. In: AGU Fall Meeting Abstracts. San Francisco, CA, USA: American Geophysical Union.

Guenthner WR, Reiners PW, Tian Y. 2014. Interpreting date-eU correlations in zircon (U-Th) /He datasets: A case study from the Longmen Shan, China. Earth and Planetary Science Letters, 403, 328–339. doi: 10.1016/j.epsl.2014.06.050.

Guo L, Wang T, Zhang JJ, Liu J, Qi GW, Li JB. 2012. Evolution and time of formation of the Hohhot metamorphic core complex, North China: New structural and geochronological evidence. International Geology Review, 54(11), 1309–1331. doi: 10.1080/00206814.2011.638438.

Guo XQ. 2022. The characteristics of tectonic evolution during Mesozoic and Cenozoic Era in Taiyueshan uplift area, central and southern Shanxi province. Taiyuan, Taiyuan University of Technology, Master thesis, 43–59 (in Chinese with English abstract).

Huang ZG, Ren ZL, Gao LG. 2016. Evidence from detrital zircon and apatite fission track for tectonic evolution since Cretaceous in southeastern margin of Ordos basin. Chinese Journal of Geophysics, 59(10), 3753–3764 (in Chinese with English abstract). doi: 10.6038/cjg20l61020.

Imayama T, Koh Y, Aoki K , Saneyoshi M, Yagi K, Aoki S, Terada T, Sawada Y, Ikawa C, Ishigaki S. 2019. Late Permian to Early Triassic back-arc type volcanism in the southern Mongolia volcano-plutonic belt of the Central Asian Orogenic Belt: Implication for timing of the final closure of the Paleo-Asian Ocean. Journal of geodynamics, 131(Nov.), 1–15. doi: 10.1016/j.jog.2019.101650.

Jiang L, Qiu Z, Wang QC, Guo YS, Wu CF, Wu ZJ, Xue ZH. 2016. Joint development and tectonic stress field evolution in the southeastern Mesozoic Ordos Basin, west part of North China. Journal of Asian Earth Sciences, 127, 47–62. doi: 10.1016/j.jseaes.2016.06.017.

Jin RS, Feng XX, Teng XM, Nie FJ, Cao HY, Hou HQ, Liu HX, Miao PS, Zhao HL, Chen LL, Zhu Q, Zhou XX. 2020a. Genesis of green sandstone/mudstone from Middle Jurassic Zhiluo Formation in the Dongsheng Uranium Orefield, Ordos Basin and its enlightenment for uranium mineralization. China Geology, 3, 52–66. doi: 10.31035/cg2020002.

Jin RS, Teng XM, Li XG, Si QH, Wang W. 2020b. Genesis of sandstone-type uranium deposits along the northern margin of the Ordos Basin, China. Geoscience Frontier, 11, 215–227. doi: 10.1016/j.gsf.2019.07.005.

Jolivet M, Brunel M, Seward D, Xu Z, Yang J, Roger F, Tapponnier P, Malavieille J, Arnaud N, Wu C. 2001. Mesozoic and Cenozoic tectonics of the northern edge of the Tibetan plateau, fission-track constraints. Tectonophysics, 343 (1–2), 111–134. doi: 10.1016/S0040-1951(01)00196-2.

Ketcham RA. 2005. Forward and inverse modeling of low-temperature thermochronometry data. Reviews in Mineralogy & Geochemistry, 58, 275–314. doi: 10.2138/rmg.2005.58.11.

Li B. 2019. Thrust structure and its effect on hydrocarbon in the western margin of Ordos Basin. Xi'an, Northwest University, Master thesis, 57–60 (in Chinese with English Abstract).

Li JY. 2009. Cycles and stages of geological history of China Mainland. Geology in China, 26(3), 504–527 (in Chinese with English abstract).

Li S, Chung SL, Wilde SA, Wang T, Xiao WJ, Guo, QQ. 2016. Linking magmatism with collision in an accretionary orogen. Scientific Reports, 6, 25751. doi: 10.1038/srep25751.

Li SZ, Suo YH, Li XY, Zhou J, Santosh M, Wang PC, Wang GZ, Guo LL. 2019. Mesozoic tectono-magmatic response in the East Asian ocean-continent connection zone to subduction of the Paleo-Pacific Plate. Earth-Science Reviews, 192, 91–137. doi: 10.1016/j.earscirev.2019.03.003.

Li ZD, Duo XF, Li XG, Zhang F, Zhang J, Chen JQ, Wang JY. Wen SB. 2020. Geochemical characteristics zircon U-Pb age and Hf isotope of the gabbro in the Huanghuatan Cu-Ni deposit Darhan Muminggan Joint Banner Inner Mongolia. Geological Bulletin of China, 39(4), 491–502 (in Chinese with English abstract). doi:CNKI:SUN:ZQYD.0.2020-04-008.

Liu CY, Qiu XW, Wu B L, Zhao HG. 2009. Subdivisions of the Central-East Asia multi-energy minerals metallogenetic domain and types of those basins. Energy Exploration Exploitation, 27(3), 153–166 (in Chinese with English Abstract). doi:CNKI:SUN:XJSD.0.2009-04-007.

Liu CY, Wu BL, 2016. Mechanism and Enrichment Distribution of Hydrocarbon, Coal and Uranium Coexisting with Basin: Accumulation and Distribution Theory and Progress. Beijing, Science Press, 73–176 (in Chinese with English abstract).

Liu CY, Zhao HG, Gui XJ, Yue LP, Zhao JF, Wang JQ. 2006. Space-time coordinate of the evolution and reformation and mineralization response in Ordos Basin. Acta Geologica Sinica, 80, 617–638 (in Chinese with English abstract). doi: 10.3321/j.issn:0001-5717.2006.05.001.

Liu J, Zhang JJ, Guo L, Qi GW. 2014. $^{40}Ar/^{39}Ar$ dating of the detachment fault of the Hohhot metamorphic core complex, Inner Mongolia, China. Acta Petrologica Sinica, 30(7), 1899–1908 (in Chinese with English abstract). doi:CNKI:SUN:YSXB.0.2014-07-006.

Liu JH, Zhang PZ, Zheng DW, Wan JL, Wang WT, Du P, Lei QY. 2010. Pattern and timing of late Cenozoic rapid exhumation and uplift of the Helan Mountain, China. Science China-Earth Science, 53(3), 345–355. doi: 10.1007/s11430-010-0016-0.

Liu K, Zhang J, Wilde SA, Zhou J, Wang M, Ge M, Wang J, Ling Y. 2017. Initial subduction of the Paleo-Pacific Oceanic plate in NE

China: Constraints from whole-rock geochemistry and zircon U-Pb and Lu-Hf isotopes of the Khanka Lake granitoids. Lithos, 274–275, 254–270. doi: 10.1016/j.lithos.2016.12.022.

Liu S, Su S, Zhang G. 2013. Early Mesozoic basin development in North China: Indications of cratonic deformation. Journal of Asian Earth Sciences, 62, 221–236. doi: 10.1016/j.jseaes.2012.09.011.

Liu WS, Qin MK, Qi FS, Xiao SQ, Wang ZM. 2008. Analysis on the Meso-Neozoic subsidence and uplift history of the periphery of Ordos basin using apatite fission track. Uranium Geology, 24(4), 221–226 (in Chinese with English abstract). doi: doi: 10.3969/j.issn.1000-0658.2008.04.006.

Liu YF, Nie FJ, Jiang SH, Xi Z, Zhang ZG, Xiao W, Zhang K, Liu Y. 2011. Ore-forming fluid characteristics and ore genesis of Chaganhua porphyry molybdenum deposit in Central Inner Mongolia, China. Journal of Jilin University (Earth Science Edition), 41(6), 1794–1805 (in Chinese with English abstract). doi: 10.3969/j.issn.1671-5888.2011.06.014.

Liu YQ, Kuang HW, Peng N, Xu H, Zhang P, Wang NS, An W. 2015. Mesozoic basins and associated palaeogeographic evolution in North China. Journal of Palaeogeography, 4(2), 189–202. doi: 10.3724/SP.J.1261.2015.00073.

Liu ZH, Xu ZY, Yang ZS. 2003. Indosinian tectonic movement in Daqingshan region in Inner Mongolia. Geological Reviews, (5), 457–463 (in Chinese with English abstract). doi: 10.1016/S0955-2219(02)00073-0.

Lu YP, Yu S, Zhang YQ, Zhang JF. 2015. Tectonic evolution and chronology constrains of Langshan region in Inner Mongolia autonomous. Gansu Geology, (2), 24–29 (in Chinese with English abstract). doi:CNKI:SUN:GSDZ.0.2015-02-005.

Ma XJ, Liang JW, Li JX, Jia WH, Tao WX, Liu YL, Liu XF. 2019. Meso-Cenozoic tectonic uplift and evolution of Central and Western Ordos Basin. Northwestern Geology, 52(4), 127–136 (in Chinese with English Abstract). doi:CNKI:SUN:XBDI.0.2019-04-013.

Ma YF, Liu YJ, Peskov A, Wang Y, Song WM, Zhang YJ, Qian C, Liu TJ, 2022. Paleozoic tectonic evolution of the eastern Central Asian Orogenic Belt in NE China. China Geology, 5, 555–578. doi: 10.31035/cg2021079.

Ma YS. 2001. The evolution of Mesozoic-Cenozoic basin-mountain structure in the east Yanshan area and Xialiaohe basin. Journal of Geomechanics, 7(1), 80–89 (in Chinese with English Abstract). doi: 10.3969/j.issn.1006-6616.2001.01.010.

Malusà GM, Fitzgerald GP. 2019. Fission-track Thermochronology and Its Application to Geology. Springer, Switzerland, 1–393.

Miao PS, Jin RS, Li JG, Zhao HL, Chen LL, Chen Y, Si QH. 2020. The first discovery of a large sandstone-type uranium deposit in aeolian depositional environment. Acta Geologica Sinica (English Edition), 94(2), 583–584. doi: 10.1111/1755-6724.14518.

Murray KE, Orme DA, Reiners PW. 2014. Effects of U-Th-rich grain boundary phases on apatite helium ages. Chemical Geology, 390, 135–151. doi: 10.1016/j.chemgeo.2014.09.023.

Nie FJ, Jiang SH, Liu Y, Hu P. 2005. Re-discussions on the time limitation of gold mineralization occurring within the Hadamengou deposit, south-central Inner Mongolia autonomous region. Acta Petrologica Sinica, 21(6), 1719–1728 (in Chinese with English abstract). doi: 10.1111/j.1440-1789.2005.00601.x.

Nie FJ, Jiang SH, Su XX, Wang XL. 2002. Geological features and origin of gold deposits occurring in the Baotou-Bayan Obo district, south-central Inner Mongolia, People's Republic of China. Ore Geology Reviews, 20(3–4), 139–169. doi: 10.1016/S0169-1368(02)00069-0

Peng ZM, Peng SM, Wu ZP, Li W, Kong X. 2009. Basin pattern and evolution of Triassic in North China. Journal of Xi'an Shiyou University (Natural Science Edition) 24(2), 34–38 (in Chinese with English abstract).

Qiao JX. 2013. The Tectonic Evolution and Oil-gas Effect of Meso-Cenozoci Yimeng Uplift. Xi'an, Northwest University, Master thesis, 45–56 (in Chinese with English abstract).

Reiners PW, Nicolescu S. 2006. Measurement of parent nuclides for (U-Th) /He chronometry by solution sector ICP-MS, ARHDL Report 1. Tucson, Arizona: University of Arizona.

Reiners PW, Farley KA, Hickes HJ, 2002. He diffusion and (U-Th)/He thermochronometry of zircon: Initial results from Fish Canyon Tuff and Gold Butte. Tectonophysics, 349 (1–4), 297–308. doi: 10.1016/s0040-1951(02)00058-6.

Reiners PW. 2005. Zircon (U-Th)/He Thermochronometry. Reviews in Mineralogy & Geochemistry, 58(1), 151–179. doi: 10.2138/rmg.2005.58.6.

Reiners PW. 2009. Nonmonotonic thermal histories and contrasting kinetics of multiple thermochronometers. Geochimica et Cosmochimica Acta: Journal of the Geochemical Society and the Meteoritical Society, 73(12), 3612–3629. doi: 10.1016/j.gca.2009.03.038.

Ren XM, Zhu WB, Zhu XQ, Wang X, Luo M. 2015. Mesozoic-Cenozoic uplift exhumation history in Luliangshan Area of Shanxi: Evidences from apatite fission track. Journal of Earth Sciences and Environment, 37(4), 63–73 (in Chinese with English abstract).

Ren ZL, Cui JP, Guo K, Tian T, Li H, Wang W, Yang P, Cao ZP. 2015. Fission-track analysis of uplift times and processes of the Weibei Uplift in the Ordos Basin. Chinese Science Bulletin, 60, 1298–1309 (in Chinese with English abstract). doi: 10.1360/N972014-00617.

Ren ZL, Qi K, Liu RC, Liu RC, Cui JP, Chen ZP, Zhang YY, Yang GL, Ma S. 2020. Dynamic background of Early Cretaceous tectonic thermal events and its control on various mineral accumulations such as oil and gas in the Ordos Basin. Acta Petrologica Sinica, 36(4), 1213–1234 (in Chinese with English abstract). doi: 10.18654/2095-8927/015.

Ren ZL, Zhang S, Gao SL. 2006. Relationship between thermal history and various energy mineral deposits in Dongsheng area, Yimeng uplift. Oil & Gas Geology, 27(2), 187–193 (in Chinese with English abstract). doi: 10.11743/ogg20060208.

Shi W, Zhang YQ, Ma YS, Liu G, Wu L. 2006. Formation and modification history of the Liupanshan basin on the southwestern margin of the Ordos block and tectonic stress field evolution. Geology in China, 33(5), 1066–1074 (in Chinese with English Abstract). doi: 10.3969/j.issn.1000-3657.2006.05.016.

Shuster DL, Flowers RM, Farley KA. 2006. The influence of natural radiation damage on helium diffusion kinetics in apatite. Earth and Planetary Science Letters, 249(3–4), 148161. doi: 10.1016/j.epsl.2006.07.028.

Song DF, Glorie S, Xiao WJ, Collins AS, Gillespie J, Jepson G, Li YC. 2018. Tectono-thermal evolution of the southwestern Alxa tectonic belt, NW China, constrained by apatite U-Pb and fission track thermochronology. Tectonophysics, 722(1), 577–594. doi: 10.1016/j.tecto.2017.11.029.

Spiegel C, Kohn B, Belton D, Berner Z, Gleadow A. 2009. Apatite (U-Th-Sm)/He thermochronology of rapidly cooled samples: The effect of He implantation. Earth and Planetary Science Letters, 285(1–2), 105–114. doi: 10.1016/j.epsl.2009.05.045.

Stevens T, Carter A, Watson TP, Vermeesch P, Andò S, Bird AF, Lu H, Garzanti E, Cottamf MA, Sevastjanova I. 2013. Genetic linkage between the Yellow River, the Mu Us desert and the Chinese Loess Plateau. Quaternary Science Reviews, 78, 355–368. doi: 10.1016/j.quascirev.2012.11.032.

Sun JB, Chen W, Yu S, Shen Z, Tian YT. 2017. Study on zircon (U-Th)/He dating technique. Acta Petrologica Sinica, 33(6), 1947–1956 (in Chinese with English abstract).

Sun JB, Sun TF, Chen W, Yu S, Yin JY, Li C, Zhang Y, Liu XY. 2015. Thermo-tectonic evolution history of Hongyuntan area, eastern

Tianshan, Xinjiang: Constrained from Ar–Ar and (U-Th) /He dating. Acta Petrologica Sinica, 31(12), 3732–3742 (in Chinese with English abstract). doi:CNKI:SUN:YSXB.0.2015-12-017.

Sun JB. 2008. The Meso-Cenozoic Tectonic Events and its Gas Accumulation Effect in the Northeastern Ordos Basin. Xi'an, Northwest University, Master thesis, 48–57 (in Chinese with English abstract).

Suo YH, Li SZ, Cao XZ, Wang XY, Somerville I, Wang GZ, Wang PC, Liu B. 2020. Mesozoic-Cenozoic basin inversion and geodynamics in East China, A review. Earth Science Reviews, 210, 103357. doi: 10.1016/j.earscirev.2020.103357.

Tang XY, Yang SC, Hu SB. 2022. Tectonic-thermal history and hydrocarbon potential of the Pearl River Mouth Basin, northern South China Sea: Insights from borehole apatite fission-track thermochronology. China Geology, 6(3), 429–442. doi: 10.31035/cg2022055.

Thomas WA. 2011. Detrital-zircon geochronology and sedimentary provenance. Lithosphere 3, 304–308. doi: 10.1130/rf.l001.1.

van Soest MC, Hodges KV, Wartho JA, Biren MB, Monteleone BD, Ramezani J, Spray JG, Thompson LM. 2011. (U-Th)/He dating of terrestrial impact structures: The Manicouagan example. Geochemistry Geophysics Geosystems, 12, Q0AA16. doi: 10.1029/2010GC003465.

Vermeesch P, Sherlock SC, Roberts NMW, Carter A. 2012. A simple method for in-situ U-Th-He dating. Geochimica et Cosmochimica Acta, 79(3), 140–147. doi: 10.1016/j.gca.2011.11.042.

Wang B, Zhao GC. 2021. Final closure of the Paleo-Asian ocean: Constraints from Permian-Triassic magmatism in the eastern segment of the Bainaimiao Arc Belt. Journal of Northwest University (Natural Science Edition), 51(6), 1019–1030 (in Chinese with English abstract). doi: 10.16152/j.cnki.xdxbzr.2021-06-008.

Wang JQ, Liu CY, Zhao HG, Zhang DD, Zattin M and Peng H. 2020. Uplift and exhumation events and thermochronological constraints at the end of Triassic in southwestern Ordos Basin. Acta Petrologica Sinica, 36(4), 1199–1212 (in Chinese with English abstract). doi: 10.18654/1000-0569/2020.04.14.

Wang SM. 2017. Ordos Basin superposed evolution and structural controls of coal forming activities. Earth Science Frontiers, 24(2), 054–063. doi: 10.13745/j.esf.yx.2016-12-11.

Wang SY, Cheng YH, Li CH, Li YF, Zhang TF, Cheng XY, Yang J. 2020. Tectonic evolution and its controls on the sandstone-type uranium mineralization in the Yimeng Uplift, constraints from apatite fission track thermochronology. Geotectonica et Metallogenia, 44(4), 682–696 (in Chinese with English abstract). doi: 10.16539/j.ddgzyckx.2020.04.010.

Wang T, Wang XX, Tian W, Zhang CL, Li WP, Li S. 2009. North Qinling Paleozoic granite associations and their variation in space and time: Implications for orogenic processes in the orogens of central China. Science in China Series D, 52, 1359–1384. doi: 10.1007/s11430-009-0129-5.

Wang T, Zhang JJ, Li S, Tong Y, Guo L, Zhang XW, Huang H, Zhang L, Xue HM. 2022. Distinctive spatial-temporal evolution of Late Paleozoic to Mesozoic magmatic systems in Northeast Asia: Evidences for identification of the extent and superposition of multiple plate tectonic regimes. Earth Science Frontiers, 29(2), 028–044. doi: 10.13745/j.esf.sf.2022.2.5.

Wang XX, Wang T, Zhang CL. 2015. Granitoid magmatism in the Qinling orogen, central China and its bearing on orogenic evolution. Science in China Series D. 58, 1497–1512. doi:CNKI:SUN:JDXG.0.2015-09-003.

Wang Y, Dong S, Shi W, Chen XH, Jia LM. 2017. The Jurassic structural evolution of the western Daqingshan area, eastern Yinshan belt, North China. International Geology Review, 59(15), 1885–1907. doi: 10.1080/00206814.2017.1300784.

Warnock AC, Zeitler PK, Wolf RA, Bergman SC. 1997. An evaluation of low-temperature apatite (U-Th)/He thermochronometry. Geochimica et Cosmochimica acta, 61(24), 5371–5377. doi: 10.1016/s0016-7037(97)00302-5.

Wilde SA. 2015. Final amalgamation of the Central Asian Orogenic Belt in NE China: Paleo-Asian Ocean closure versus Paleo-Pacific plate subduction-A review of the evidence. Tectonophysics, 662, 345–362. doi: 10.1016/j.tecto.2015.05.006.

Wolf RA, Farley KA, Kass DM. 1998. Modeling of the temperature sensitivity of the apatite (U-Th)/He thermochronometer. Chemical Geology, 148, 105–114. doi: 10.1016/S0009-2541(98)00024-2.

Wu D, Li S, Chew D, Liu TY, Guo DH. 2021. Permian-Triassic magmatic evolution of granitoids from the southeastern Central Asian Orogenic Belt: implications for accretion leading to collision. Science China (Earth Sciences), 64, 788–806. doi: 10.1007/s11430-020-9714-5.

Wu HH, Huang H, Zhang Z, Wang T, Wang W. 2020. Geochronology, geochemistry, mineralogy and metallogenic implications of the Zhaojinggou Nb-Ta deposit in the northern margin of the North China Craton, China. Ore Geology Reviews, 125, 103692. doi: 10.1016/j.oregeorev.2020.103692.

Wu ZH. 2003. Uplift History of the Daqing Mountain since the Late Cretaceous. Acta Geoscientica Sinica, 24(3), 205–210 (in Chinese with English abstract). doi: 10.3321/j.issn:1006-3021.2003.03.002.

Xiao WJ, Windley BF, Sun S, Li J, Huang BC, Han CM, Yuan C, Sun M, Chen HL. 2015. A tale of amalgamation of three Perm-Triassic collage systems in Central Asia: Oroclines, sutures, and terminal accretion. Annual Review of Earth and Planetary Sciences, 43, 477–507. doi: 10.1146/annurev-earth-060614-105254.

Xu QQ, Ji JQ, Zhao WT, Yu XJ. 2017. Uplift exhumation history of Daqing Mountain, Inner Mongolia, since Late Mesozoic. Acta Scientiarum Naturalium Universitatis Pekinensis, 53(1), 57–65 (in Chinese with English abstract). doi: 10.13209/j.0479-8023.2016.096.

Xu WL, Pei FP, Wang F, Meng E, Ji WQ, Yang DB, Wang W. 2013. Spatial-temporal relationships of Mesozoic volcanic rocks in NE China: Constraints on tectonic overprinting and transformations between multiple tectonic regimes. Journal of Asian Earth Sciences, 74, 167–193. doi: 10.1016/j.jseaes.2013.04.00.3.

Xu ZQ, Yang JS, Li HB, Zhang JX, Zeng LS, Jiang M. 2006. The Qinghai-Tibet plateau and continental dynamics: A review on terrain tectonics, collisional orogenesis, and processes and mechanisms for the rise of the plateau. Geology in China, 33(2), 221–238 (in Chinese with English Abstract). doi: 10.3969/j.issn.1000-3657.2006.02.001.

Xu ZY, Liu ZH, Yang ZS. 2001. Mesozoic orogenic movement and tectonic evolution in Daqingshan region, Inner Mongolia. Journal of Changchun University of Science and Technology, 31(4), 317–322 (in Chinese with English abstract). doi:CNKI:SUN:CCDZ.0.2001-04-001.

Yang MH, Li L, Zhou J, Jia HC, Sun X, Qu XY, Zhou D, Gong T, Ding C. 2015. Mesozoic structural evolution of the Hangjinqi area in the northern Ordos Basin, North China. Marine and Petroleum Geology, 66(4), 695–710. doi: 10.1016/j.marpetgeo.2015.07.014.

Yang MH, LiL, Zhou J, Qu XY, Zhou D. 2013. Segmentation and inversion of the Hangjinqi fault zone, the northern Ordos basin (north China). Journal of Asian Earth Sciences, 70–71(Jul.), 64–78. doi: 10.1016/j.jseaes.2013.03.004.

Yang MH, Liu CY, Zeng P, Bai H, Zhou J. 2012. Prototypes of Late Triassic Sedimentary Basins of North China Craton (NCC) and Deformation Pattern of Its Early Destruction. Geological Review, (1), 1–18 (in Chinese with English abstract). doi: 10.1007/s11783-011-0280-z.

Yang XC. 2018. Uplift Process of the Western Section of Yinshan from Mesozoic to Cenozoic Period and Its Geological Implications. Chinese Academy of Geological Sciences, Doctoral thesis, 27–34 (in

Chinese with English abstract).

Yi ZY, Yang SL, Meert JG, Ma XX. 2022. Paleomagnetism of late Cretaceous dykes in the Gangdese belt: New constraints on the position and structure of the southern margin of Asia prior to the India-Asia collision. China Geology, 6, 269–284. doi: 10.31035/cg2022077.

Yu Q, Ren ZL. 2008. Comparison of Geothermal Fields in the Huangling and Dongsheng Areas, Ordos Basin. Journal of Jilin University (Earth Science Edition), 38(6), 933–936 (in Chinese with English abstract). doi: 10.13278/j.cnki.

Yu RA, Wang SB, Zhu Q, Si QH, Teng XM, Liu XX, Liu HN, Tang YX. 2021. Zircon U-Pb ages and provenance characteristics of the Zhiluo Formation sandstones and the formation background of the uranium deposit in Huangling area, Ordos Basin, China. China Geology, 4, 600–615. doi: 10.31035/cg2021006.

Zattin M, Wang X. 2019. Exhumation of the western Qinling Mountain range and the building of the northeastern margin of the Tibetan Plateau. Journal of Asian Earth Sciences, 177(JUN.15), 307–313. doi: 10.1016/j.jseaes.2019.04.002.

Zhang C, Neubauer F, Liu ZH, Cui FH, Guan QB. 2020. Final-Stage magmatic record of Paleo-Asian oceanic subduction? Insights from Late Permian to Early Triassic intrusive rocks in the Yanbian Area, Easternmost Central Asian Orogenic Belt. Minerals, 10(9), 799. doi: 10.3390/min10090799.

Zhang HD, Liu JC, Fayek M. 2021. Multistage mineralization in the Haoyaoerhudong gold deposit, Central Asian Orogenic Belt: Constraints from the sedimentary-diagenetic and hydrothermal sulfides and gold. Geoscience Frontiers, 12(2), 587–604. doi: 10.1016/j.gsf.2020.08.003.

Zhang HT, So CS, Yun ST. 1999. Regional geologic setting and metallogenesis of central inner mongolia, China: Guides for exploration of mesothermal gold deposits. Ore Geology Reviews, 14(2), 129–146. doi: 10.1016/S0169-1368(98)00019-5.

Zhang JJ, Qi GW, Guo L, Liu J. 2009. $^{40}Ar/^{39}Ar$ dating of the Mesozoic thrusting in Daqingshan thrust-nappe system, Inner Mongolia, China. Acta Petrologica Sinica, 25, 609–620 (in Chinese with English abstract). doi: 10.1016/S1874-8651(10)60080-4.

Zhang RR. 2015. Geochemistry and Geochronology Research of the Ore-forming Intrusive Body in the Chagandeersi Molybdenum Deposit, Inner Mongolia. Wuhan, China University of Geosciences, Master thesis, 33–44 (in Chinese with English abstract).

Zhang WL. 2016. Tectonic Dynamothermal Transition of the Meso-Cenozoic and Its Constraints on Coupled Metallogeneses in the Northeast Ordos Basin. Xi'an, Northwest University, Mater thesis, 30–36 (in Chinese with English abstract).

Zhang XH, Zhai MG. 2010. Magmatism and its metallogenetic effects during the Paleozoic continental crustal construction in northern North China: An overview. Acta Petrologica Sinica, 26(5), 1329–1341 (in Chinese with English abstract). doi: 10.1107/S1600536802007420.

Zhang XM, Xu WL, Sun C, Feng W, Yang DB. 2019. Geochronology and geochemistry of Early Mesozoic magmatism in the northeastern North China Craton: Implications for tectonic evolution. Gondwana Research, 67, 33–45. doi: 10.1016/j.gr.2018.10.013.

Zhang YM, Gu XX, Dong SY, Cheng WB, Huang ZQ, Li FL, Yang WL. 2011. Zircon U-Pb and molybdenite Re-Os dating for the Xishadegai molybdenum deposit in Inner Mongolia and its geological significance. Journal of Mineralogy & Petrology, 31(2), 33–41 (in Chinese with English abstract). doi: 10.1007/s11589-011-0776-4.

Zhang YQ, Chen XH, Zhang J, Shao ZG, Ding WC, Guo XG, Wang DR, Gu WP, Wang Y, Xu SL, Qin X. 2019. Discussion on the initial timing of the Indosinian movement in the Ordos basin and the Sichuan basin: Constraints from growth strata evidence. Geology in China, 46(5), 1021–1038 (in Chinese with English abstract). doi: 10.12029/gc20190505.

Zhang YQ, Liao CZ, 2006. Transition of the Late Mesozoic-Cenozoic tectonic regimes and modification of the Ordos Basin. Geology in China, 33, 28–36 (in Chinese with English abstract).

Zhang YQ, Liao CZ, Shi W, Zhang T, Guo FF. 2007. Jurassic deformation in and around the Ordos Basin, North China. Earth Science Frontiers, 14(2), 182–196. doi: 10.1016/S1872-5791(07)60016-5.

Zhang YQ, Shi W, Dong SW. 2011. Changes of Late Mesozoic tectonic regimes around the Ordos Basin (North China) and their geodynamic implications. Acta Geological Sinica, 85(6), 1254–1276 (in Chinese with English abstract). doi: 10.1111/j.1755-6724.2011.00586.x.

Zhao JF, Liu CY, Huang L, Zhang DD, Wang D, Wang D. 2020. Paleogeography reconstruction of a multi-stage modified intra-cratonic basin—a case study from the Jurassic Ordos Basin, Western North China Craton. Journal of Asian Earth Sciences 190, 104–191. doi: 10.1016/j.jseaes.2019.104191.

Zhao XC, Liu CY, Zhao Y, Deng H, Zhang QH, 2016. Response of the Ningnan Area to the Eocene peripheral rifting breakup event of the Ordos Basin. Geological science and Technology Information, 35(6), 24–29 (in Chinese with English Abstract). doi:CNKI:SUN:DZKQ.0.2016-06-005.

Zhao Y, Zhai MG, Chen H, Zhang SH. 2017. Paleozoic-early Jurassic tectonic evolution of North China Craton and its adjacent orogenic belts. Geology in China, 44(1), 44–60 (in Chinese with English abstract). doi: 10.12029/gc20170104.

Zheng DW, Zhang PZ Wan JL, Yuan DY, Zhang GL, Li CY, Yin GM, Zhang GL, Wang ZC, Ming W, Chen J. 2006. Rapid exhumation at ~ 8 Ma on the Liupan Shan thrust fault from apatite fission-track thermochronology: Implications for growth of the northeastern Tibetan Plateau margin. Earth and Planetary Science letters, 248, 198–208. doi: 10.1016/j.epsl.2006.05.023.

Zheng YD, Davis GA, Wang Z, Darby BJ, Hua YG. 1998. Major thrust sheet in the Daqing Shan Mountains, Inner Mongolia, China. Science in China (Series D), (5), 553–560 (in Chinese with English abstract). doi: 10.1007/BF02877747.

Zhou ZY. 2014. Low Temperature Thermochronology: Principles & Applications. Beijing, Science Press, 1–230 (in Chinese).

Zhu G, Chen Y, Jiang DZ, Lin SZ. 2015. Rapid change from compression to extension in the North China Craton during the Early Cretaceous, Evidence from the Yunmengshan metamorphic core complex. Tectonophysics, 656, 91–110. doi: 10.1016/j.tecto.2015.06.009.

Zhu RX, Xu YG. 2019. The subduction of the west Pacific plate and the destruction of the North China Craton. Science China Earth Sciences, 62, 1340–1350. doi: 10.1007/s11430-018-9356-y.

Zou HP, Zhang K, Li G. 2008. Cretaceous tectono-thermal event in the Ordos Block: An Ar-Ar chronological evidence from basalt at Hangjin Banner, Inner Mongolia, North China Craton. Geotectonica et Metallogenia, 32(3), 360–364 (in Chinese with English abstract). doi: 10.3969/j.issn.1001-1552.2008.03.014.